



Norwegian University of
Science and Technology

Wing impactor for testing of aviation masts

Jørgen Johnsen

Mechanical Engineering

Submission date: February 2016

Supervisor: Terje Rølvåg, IPM

Norwegian University of Science and Technology
Department of Engineering Design and Materials

THE NORWEGIAN UNIVERSITY
OF SCIENCE AND TECHNOLOGY
DEPARTMENT OF ENGINEERING DESIGN
AND MATERIALS

**MASTER THESIS AUTUMN 2015
FOR
STUD. TECHN. JØRGEN JOHNSEN**

WING IMPACTOR FOR TESTING OF AVIATION MASTS

Vinge impactor for testing av flyplass master

A NLR soft wing impactor was used for physical testing of Finnish, Swedish, Norwegian and Canadian aviation masts between 1976 and 2000. With the exception of one experiment at MIRA presented at the 2014 JAFSG meeting by Griffith, very few physical tests have been reported after 2000. Griffith did not use a soft wing impactor but the semicircular tube proposed in the ICAO standard. The results were dominated by noise due to resonance problems and the author therefore recommended a deformable soft impactor in future tests. The same type of problems have been observed and reported in virtual and physical tests by the supervisor.

However, The ICAO standard recommends rigid impactors, but there are reasons to believe there is a big difference to be hit by a rigid impactor compared to a soft wing impactor. They both weight 3 tons (the mass of a Beechcraft Model 80 Queen Air) and they shall hit the mast at a speed of 140 km/h according to the ICAO rules. The main difference is the initial peak force that occurs when an impactor with a 22 mm steel front plate versus a 0.8 mm aluminum sheet structure hits rigid components like hinges on an aviation mast.

Simulations performed by the supervisor prove that rigid impactors generate initial reaction forces far above the ICAO limits when they hit a typical aluminum mast. They are still being used due to low building and testing costs.

These are strong arguments for this master project, e.g. the development and use of a standard but simple soft wing impactor. Unfortunately, there is no standard soft impactor and many variants have been used by different mast manufacturers. The documented crash results are therefore not directly comparable. The ICAO rules do neither provide guidelines for soft impactors nor restrict the use of data filtering which has a major impact on the peak forces.

The main objective with this project (and master) is therefore to document, benchmark and qualify a simplified low cost version of the NLR soft impactor. The

Tasks to be completed:

1. Study and document the ICAO and FAA crash safety requirements for aviation masts.
2. Study the current soft wing impactor design and properties proposed by NLR
3. Identify and model simplified low cost soft impactors assumed to match the dynamic properties of the NLR wing impactor. Perform crash tests of the simple soft impactors based on a selected (dummy) aviation mast.
4. Identify and document the properties of the most promising simple soft wing impactor. Compare the crash properties and costs with the original NLR soft wing impactor.

Formal requirements:

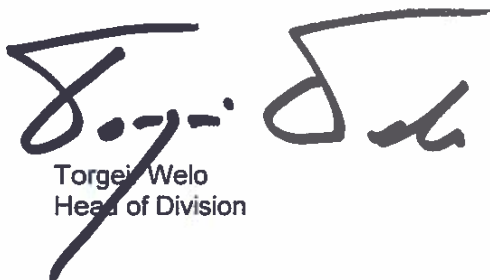
Three weeks after start of the thesis work, an A3 sheet illustrating the work is to be handed in. A template for this presentation is available on the IPM's web site under the menu "Masteroppgave" (<http://www.ntnu.no/ipm/masteroppgave>). This sheet should be updated one week before the master's thesis is submitted.

Risk assessment of experimental activities shall always be performed. Experimental work defined in the problem description shall be planned and risk assessed up-front and within 3 weeks after receiving the problem text. Any specific experimental activities which are not properly covered by the general risk assessment shall be particularly assessed before performing the experimental work. Risk assessments should be signed by the supervisor and copies shall be included in the appendix of the thesis.

The thesis should include the signed problem text, and be written as a research report with summary both in English and Norwegian, conclusion, literature references, table of contents, etc. During preparation of the text, the candidate should make efforts to create a well arranged and well written report. To ease the evaluation of the thesis, it is important to cross-reference text, tables and figures. For evaluation of the work a thorough discussion of results is appreciated.

The thesis shall be submitted electronically via DAIM, NTNU's system for Digital Archiving and Submission of Master's theses.

The contact person is [navn på veileder i utlandet, bedrift eller lignende].



Torgeir Welo
Head of Division



Terje Rølvåg
Professor/Supervisor



NTNU
Norges teknisk-
naturvitenskapelige universitet
Institutt for produktutvikling
og materialer

Abstract

Operations at airfields require the use of certain visual and nonvisual aids in order to operate at nearly any weather condition. Some of these, such as the approach lighting system are positioned in such a way as to present a hazard to aircraft safety. The support structure of the approach lighting system are required to be frangible. The frangibility of a mast determines through a full-scale dynamical crash-test, where the masts deformation sequence, max impact force and energy are direct measures on its frangibility. Today's standard recommends the use of a rigid impactor to represent the wing section of a small aircraft. Simulations show however that the rigid impactor generates initial reaction forces far above the ICAO rules. The rigid impactor is still used due low production and test cost related to it. The current version of a deformable impactor is a true copy of the wing section of a small aircraft. This makes it complex and expensive to manufacture. The main objective of this thesis is therefore to develop an alternative low-cost deformable impactor for future crash-tests.

Through studying test results from previous quasi-static compression tests of the current standard wing impactor, I define and describe a characteristic dynamic force-response in which the new impactor must mimic. Several concepts has been evaluated, where a simplification of the current soft wing impactor showed to provide the best solution with respect to both dynamic response and cost. A detailed version of the concept has been proposed.

To test the chosen products dynamical responses, a quasi-statical compression test and a dynamical compression test has been performed in ABAQUS. The impactor was compressed using a rigid intruder with a representative cross-section of a typical aviation mast. The quasi-static compression test was performed with an intruder speed of 50 mm/min and the dynamical with an intruder speed of 140 km/h. A bi-linear material model and a non-linear material model was chosen to investigate the effects of strain hardening on the post-yielding behavior.

The results from the quasi-static compression tests showed promising results with regards to deformation modes, but the strength of the impactor was a little low. This could be increased by small alteration of geometry. The model showed to be sensitive to strain hardening, which had a negative effect and altered deformation modes slightly. The dynamical compression test showed to be in very good relation to the current soft wing impactor, both in deformation modes and recorded force levels. The model was not sensitive to strain hardening in the dynamical analysis. These results must however be considered only as an indication on the impactors properties, as a there are great uncertainties related to the material modelling used. Optimization of the concept and further testing and validation is necessary before this product can be put to use.

Sammendrag

Drift av flyplasser krever tilstedeværelse av ulike visuelle og ikke-visuelle hjelpemidler for å kunne operere trygt under nærmest enhver vær-situasjon. Noen av disse, som innseilingslys foran og rundt rullebaner er posisjonert slik at de utgjøre en fare for flysikkerheten. I den forbindelse settes det krav til støttestrukturen om at de skal være frangible. En masts frangibilitet avgjøres gjennom fullskala kollisjonstester hvor støttestrukturens deformasjons-sekvenser, maksimal kollisjonskraft og konsumert energi er direkte mål på dets frangibilitet. Dagens standard spesifiserer at et rigid testverktøy skal brukes til å simulere en faktisk fly-vinge i kollisjonstester. Simuleringer viser at disse impactorene generer initielle reaksjonskrefter langt over det som er satt som maks krav. De benyttes allikevel grunnet lave kostnader ved produksjon og testing. Dagens løsning for deformerbare testverktøy er en tro kopi av en faktisk fly-vinge, og fremstår som meget komplisert både i utforming og produksjon. Målet med denne oppgaven har derfor vært å utvikle en alternativ lavkostnad deformerbare testverktøy for bruk i fremtidige kollisjonstester.

Gjennom å studere testresultater fra tidligere utførte kvasi-statiske kompresjonstester av det nåværende deformerbare impactoren, definerer jeg og beskriver en karakteristisk dynamisk kraftrespons som det nye produktet må gjenspeile. Flere konsepter har blitt utviklet og evaluert, hvorpå en forenklet utgave av dagens løsning vist å være den beste løsning både med tanke på kostnader og dynamiske egenskaper.

For å teste og validere om det valgte produktet innehar de antatte mekaniske og dynamiske har det blitt gjort kompresjonstester i form av kvasi-statiske og en dynamiske simuleringer i ABAQUS. Testene bestod i å komprimere impactoren med et rigid testverktøy som har representativt tverrsnitt til en typisk flyplassmast. Kompresjonen ble utført med en hastighet på 50 mm/min og 140 km/h på de quasistatiske og dynamiske testene henholdsvis. To material modeller har blitt brukt for å undersøke modellens sensitivitet mot «strain hardening»

Resultatene fra de kvasi-statiske kompresjonstestene viste en lovende deformasjonssekvens med dertilhørende kraft-deformasjons respons. Styrken til det foreslåtte oppsettet ble registrert til å være noe lavere enn forespeilt, men kan økes til ønsket nivå med små endringer. De kvasistatiske analysene viste derimot at modellen var sensitiv for «strain hardening», og deformasjonsekvensene ble endret. Resultatene fra de dynamiske analysene samsvarer svært godt med den dynamiske responsen til det eksisterende produktet. Disse resultatene kan dog kun tolkes som en indikasjon på produktets dynamiske egenskaper, da det er knyttet mye usikkerhet til materialmodellen brukt i analysen. Optimalisering av konseptet og ytterligere testing og validering er nødvendig før produktet kan tas i bruk.

Preface

This report is written at the the Norwegian University of Science and Technology, department of Engineering design and materials. It is the product of the work done in the fall of 2015, as the final part of a five-year masters degree programme and counts as 30 credit points. The report aims at developing new test tools for physical crash testing of frangible aviation masts, and is intended for personell with special interest in the field of frangible structural components.

As a mechanical engineer student at the insitute of engineering design on NTNU, this project was a good mix a lot of the subjects taken during the course of my education. With product development as a driving factor in the project, it was intereseting to see how it could be used to solve complex crash. The world of crash analysis was totally new to me as i started this project, and a lot of time was used to understand the task at hand and to learn about modeling and performing a crash tests in an FE-code.

I would like to thank Professor Terje Rølvåg for all the guidance and support in the development of the products. I would also like to thank Staff Engineer Halvard Støwer for providing the necessary computer hardware and software for the numerical calculations in this project.

Trondheim 03.01.2016

Jørgen Johnsen

Contents

1	Introduction	1
1.1	Background	1
1.2	Purpose of this paper	2
1.3	Method	2
2	Testing for frangibility	5
2.1	Test procedure and setup.	6
2.2	Acceptance / rejection criteria.	7
2.3	Reference impactors	8
2.3.1	Rigid impactor	8
2.3.2	Softwing impactor	9
3	Design requirements	15
3.1	User	15
3.2	Product requirement	16
3.2.1	Structural properties	16
3.2.2	Cost	16
3.2.3	Geometry	17
3.2.4	Insensitive to eccentric loading	17
3.2.5	Load cells	17
4	Concept development	19
4.1	Problem decomposition	19
4.2	Search externally and internally	20
4.2.1	Subfunction 1: linear elastic	21
4.2.2	Subfunction 2: failure	21
4.2.3	Subfunction 3: constant force	21
4.3	Classification scheme	22
4.4	Concept A	23
4.5	Concept B	25
4.6	Concept C	27
4.7	Concept D	30
4.8	Proof of concept	32
4.8.1	General test setup	32
4.8.2	Material modeling	33
4.8.3	Concept A	34
4.8.4	Concept C	35
4.9	Conceptevaluation	39
5	Embodiment design	41

5.1	Mounting	41
5.1.1	Skin	41
5.1.2	Mainspar	43
5.1.3	Chosen mount principles	44
5.2	Optimization – Geometry	45
5.3	Support structure	46
5.3.1	Statical analysis	47
5.3.2	Discussion/chosen support structure	48
5.4	Final version	48
5.4.1	Assembly/production of consumables	49
6	Product simulation	51
6.1	Material modeling	51
6.2	The model	52
6.2.1	Parts/mesh/material	52
6.2.2	Assembly FEM/boundary conditions	53
6.2.3	Reducing computational costs	54
6.3	Results	55
6.3.1	Static compression test	55
6.3.2	Dynamic	58
6.4	Discussion	60
7	Conclusion and recommendations for further work	61
7.1	Conclusion	61
7.2	Further work	62
	Bibliography	63
	Attachment 1 - thesis.	
	Attachment 2 - Risk assessment master thesis.	
	Attachment 3 - Soft wing impactor dimensions.	
	Attachment 4 - Bolt loads	
	Attachment 5 - Surrogate wing impactor dimensions.	

List of Figures

2.1	Typical full-scale dynamical test-setup.	7
2.2	Rigid impactor. Photo: M.J Nead [1].	8
2.3	Beechcraft Model 80 Queen Air	9
2.4	Original NLR Soft Wing Impactor	10
2.5	Physical compression test. Photo: Wiggeraad [2]	11
2.6	Wing impactor compression test results.	12
2.7	Dynamic compression test from [3]	13
4.1	Five - step concept generation. Reproduced from [4]	19
4.2	Idealized compression response	20
4.3	Hexagonal Honeycomb with typical crush characteristics (from [5]).	22
4.4	Concept A	23
4.5	Concept B principle structure.	25
4.6	Assumed force-deflection Concept B.	26
4.7	Concept D	27
4.8	Lateral stiffening 1.	28
4.9	Lateral stiffening 2.	29
4.10	Concept D	30
4.11	Failure sequence.	30
4.12	Front beam fixture concept	31
4.13	Shearplate fixing	31
4.14	General test setup.	32
4.15	Typical stress-strain diagram for a ductile material.(from [6])	33
4.16	Concept A boundary.	35
4.17	Concept A initial compression test.	35
4.18	Concept A deformation modes.	36
4.19	Concept C final setup.	37
4.20	Concept C reaction force vs. static mast intrusion.	38
4.21	Concept C deformation modes.	39
5.1	Skin mount 1: bolting.	42
5.2	Skin mount 2: Clamping device.	42
5.3	Mount setup 3.	43
5.4	Slot mount mainspar.	43
5.5	Flange mount mainspar.	44
5.6	Main spar mount 3 configuration.	44
5.7	Finalsetup version 1.	45
5.8	Cross-section optimilization.	45
5.9	Tubular support structure.	47
5.10	Steel plate support structure.	47
5.11	Static analysis results.	48

5.12	Proposed solution assembled and exploded view.	48
5.13	Pre-cut and bent sheet.	49
5.14	Aluminum skin forming methods.	50
6.1	Material hardening models.	52
6.2	Meshed parts.	53
6.3	Assembly/test setup.	53
6.4	Constrained nodes.	54
6.5	Mass scaling definition.	54
6.6	Force versus static mast intrusion, skin thickness $t = 1$ mm	55
6.7	Force vs. static mast intrusion, $t = 0.8$ mm	56
6.8	Degree of skin stacking against main support tube.	56
6.9	Quasi - static deformation modes.	57
6.10	Comparison quasi-static tests.	58
6.11	Skin regains strength.	58
6.12	Dynamic compression forces, bi-linear material model	59
6.13	Dynamic compression forces, non-linear material model.	59

List of Tables

2.1	SWI components and typical material thickness	10
2.2	Soft wing deformation modes. Reproduced from [3]	13
4.1	Morphology table	22
4.2	Material properties [3]	34
6.1	Material properties	52

Abbreviation

ICAO	-	International Civil Aviation Organization
ADM	-	Aerodrome design manual
NLR	-	Nationaal Lucht- en Ruimtevaartlaboratorium (National Aerospace laboratory NLR)
ALS	-	Approach lighting system
SWI	-	Standard softwing impactor
FE	-	Finite element
FEA	-	Finite element analysis
FEM	-	Finite element method
CAD	-	Computer-aided design

Nomenclature

ρ	-	Density [kg/m^3]
σ_y	-	Yield stress [MPa]
E	-	Young's modulus [GPa]
σ_f	-	Foam crush strength
σ_h	-	Honeycomb crush strength
ϵ	-	Nominal strain
ε	-	True strain
ν	-	Possion's ratio

Chapter 1

Introduction

1.1 Background

Modern aircraft operations at airfields require the use of certain visual and non-visual aids such as approach lighting systems (ALS), wind direction indicators and instrument landing systems in to order operate in nearly any weather condition. Some of these aids has to be located near runways, taxiways and aprons in order to fulfill its function. Furthermore, they have to be installed at an elevated height which requires the use of a support structure with a certain strength to withstand operational loads. As a result, the support structure may present a potential risk to an aircraft during take-off, landing and ground maneuvering. The outcome of an accidental impact between such a support structure and an aircraft due to problems during take-off or landing, may well be determined by the resistance of the support structure [7].

Several fatal incidents as a direct or indirect result of an accidental impact between ALS – support structure and aircrafts has been reported. In July 1971 a Pan American World Airways Boeing 747, carrying 199 passengers struck the ALS support structure while departing the San Francisco International Airport. The aircraft sustained major structural damage, and was forced to perform an emergency landing. Two passengers were seriously injured when parts of the ALS penetrated the passenger compartment, and 27 other passengers were injured during the evacuation of the aircraft [8].

The accident with the Pan American World Airways Boeing 747 may well have been the motivation for the Federal Aviation Administration (FAA) to invest in the development and testing of a *frangible* ALS – support structure [7]. A frangible object is defined, in this respect, as an object of low mass designed to break, distort or yield on impact so as to present the minimum hazard to the aircraft [9]. In 1974, the first test effort [10] evaluating the frangibility of ALS- support structures was reported. The structures tested was an aluminum tube and, at the time, a commercially available (non-frangible) steel support structure. The ALS's was struck by an impactor mounted on a catapult carriage and the aluminum-pole proved to exhibit frangibility superior to the steel support structure. Another successful test campaign [11] was reported in 1979 of a tubular glass fiber pole which has been used for ALS support structures at airports in the US since [7].

In 1981, the "Frangible Aids Study Group" (FASG) was instigated by the International Civil Aviation Organization (ICAO) to develop international guidelines and regulation for frangible airport structures. Numerous test programmes investigating and documenting the frangibility of different mast designs were performed by mast manufacturers from Norway, Canada, Sweden, Netherlands's and Finland in the period of 1983-2003. The resulting product was Part 6 of Aerodrome design manual (ADM) [7]

which defines a set of design requirements, criteria, guidelines and test procedures for the frangibility of such aids. In the development of the frangibility requirements, two kinds of impactor has been used in full-scale dynamical impact tests; rigid and soft-impactors. The soft-impactors was a true copy of the structural elements, materials and production methods used in a small aircraft's wing. The frangibility requirements are almost entirely based on the structural damage imposed on the soft-wing impactor. However, the rigid impactor is recommended by the ADM, despite the strong recommendation of using soft-wing impactor over the years, due to assumed low production and test costs [12].

1.2 Purpose of this paper

The earlier test programs performed had to use a structurally identical impactor to an actual aircraft in order to evaluate the damage. The future test may not necessarily, hence the rigid impactor. The mechanical properties and impact response of the soft-wing impactor has been carefully studied and documented in the development of the frangibility requirements. The main objective of this project is to utilize these test results and design an alternative impactor that mimics the mechanical and dynamical response of the soft-wing impactor.

From this the projects ultimate vision and mission is stated:

Vision:

Improve flight safety.

Mission:

Lowering the threshold for the use of soft-wing impactors in evaluation of frangible aviation masts.

The project's main focus will be on the frangibility of airport lighting systems – support structure.

The project deliveries include a description of the SWI structural characteristics and an in depth conceptual phase with presentation of alternative impactors. Further should a chosen concept be further detailed and tested. Because of the time-frame of this thesis, it is considered to be a challenge to develop a final product ready for use, but is rather a possibility as to present new and innovative solutions for others to further develop and put to use.

The benefits of the work done in this project are mostly related to increased air-traffic safety. The proposed products are in the low-range production volume and the market for this type of product is limited to only a handful of mast manufacturers.

1.3 Method

In accordance with commonly used approaches at the department of Engineering design at NTNU, a systematic product development process has been employed as a mean to ensure continuous work flow and results. The work done in this project are divided into four phases:

Phase 1: Problem definition and planning.

Phase 2: Concept development.

Phase 3: Structural detailing.

Phase 4: Product verification and testing.

Phase 4 is performed through FEM numerical simulations. This method is considered not to be adequate in defining the products properties, as it require something to benchmark against. Only

physical tests can confirm the properties, so the numerical FEM rather works as a means to evaluate and find the most promising solutions.

Chapter 2

Testing for frangibility

The idea of a frangible support structure is a somewhat ambiguous statement from an engineer's point of view. On one hand, the location of which the mast is positioned requires both stiffness and strength to withstand the environmental and operation loads such as wind and jet blast from passing aircrafts. On the other hand, it should easily break, yield or distort in order to allow for the safe passage of an aircraft. In order to ensure the frangibility of any visual and non-visual aids located near runways, taxiways and aprons, the ICAO has devised a set of design requirements, criteria's, guidelines and test procedures which is depicted in the Aerodrome Design manual (ADM), part 6: Frangibility [9]. As an outline of this report, I will study and document these rules and methods for testing of frangible airport masts. As stated in the introduction chapter, the scope of this project is the approach light system support structures and thus the main focus will be on documenting the requirements and procedures related to these objects. That being said, these guidelines and regulations may also be applicable to structures of similar size and geometry but will not be taken into consideration.

An accidental impact between any fixed equipment and an aircraft may affect flight safety in three different ways according to the ADM:

1. The aircraft may lose momentum.
2. The aircraft may change direction.
3. The aircraft may suffer structural damage.

The loss of momentum is mathematically governed by the integral of force over time, which implies that both magnitude of the impact force and impact duration should be minimized. The structural damage to the aircraft is related to the amount of energy required to move the obstacle, or parts of it, out of the way. This energy is related to activation of break-away and/or failure mechanisms, plastic and/or elastic deformation of the obstacle impacted, energy required to activate break-away or failure mechanisms and the energy required to accelerate the obstacle up to at least the aircrafts velocity. The damage imposed on an aircraft is also governed by the contact area between aircraft and obstacle through which the energy transfer takes place [9]. Larger contact area prevents obstacles cutting deeply into the aircraft structure due to the distributing forces.

Frangibility of a mast can be achieved by using lightweight materials and or introducing failure mechanism and/or break-away points onto which the mast breaks, distorts or yields under impact. There are different failure mechanisms which can be applied in order to meet the frangibility requirements. Typical structures are tubular composite structures of low mass and brittle material behavior, modular designs which opens a window upon impact for the safe passage of an aircraft and one-piece designs which on impact entirely deflects away by the moving aircraft without any resistance.

The ADM states that the frangibility of any aid positioned where they are likely to be impacted by an aircraft should always be proven before the aid is considered for installation. Several methods may be applied when testing for frangibility, such as; static tests, dynamic full-scale tests and numerical simulations. The static tests are only considered adequately for structures with low mass and overall height ≤ 1.2 m. Numerical simulation has also shown to be capable of demonstrating frangibility, and with the development of sophisticated and powerful numerical solvers, the confidence in this method is increasingly. Numerical simulations are much less time-consuming and cost-effective in relation to a full-scale dynamical test and are today considered as a favorable method by engineers and mast vendors. Since the ADM was published back in 2006, the computer hardware and software has improved dramatically, allowing for much larger and advanced models to be simulated. However, the models validity greatly depends on the input values, such as material properties and dependencies. Furthermore, the numerical simulations are in some way inadequate when it comes to testing of new mast designs and materials. Therefore, numerical simulations are considered as a means of initial testing and optimization, but the only proven method is the full-scale dynamical impact test.

In the evaluation of the frangibility of an airport mast, the ADM focuses on three main areas of which must be investigated: the failure mode of the mast, impact load and energy transfer. Impact load is a rapidly changing dynamic load of short duration, typically in milliseconds. It influences the frangibility performance in two ways:

1. The maximum impact load may affect the structural integrity of the aircraft.
2. The integral of the impact load over duration of the impact leads to a change of momentum of the aircraft.

It should therefore be limited both in magnitude and duration. The energy transfer in an impact test for an ALS is directly related to point 2. as the speed at impact is considered to be constant.

For approach lighting structures which are required to be frangible, the ADM states that: "...should be designed to withstand the static and operational/survival wind loads, but should break, distort or yield readily when subjected to the sudden collision forces of a 3000-kg aircraft airborne and travelling in any direction at 140 km/h." Furthermore, the structure should not entangle with the aircraft which will prevent the aircraft from maneuvering safely. The approach lights and associated wiring should be considered as a part of the structure in the frangibility analysis.

2.1 Test procedure and setup.

The full-scale dynamical test of frangible ALS-structures should be carried out in such a manner that the conditions under which the structure might be impacted are simulated on a worst-case basis. The worst case scenario is considered to be an impact between the aircraft's wing and the ALS-structure. The test should therefore be conducted with a vehicle-driven impactor with the equivalent geometry as the wing section of a small aircraft of 3000 kg, at a constant speed of 140 km/h. A detailed description and analysis of the current reference impactors used is given in section 2.3. The impactor should be mounted on the vehicle so that it strikes the ALS-structure at a point approximately 4 m above ground level or 1 m below the top of the structure, whichever is higher. Examples of two typical test setups is shown in figure 2.1.

The mast tested should be of a production quality unit with the equipment for the service structure installed. A representative mass equivalent to the weight of the intended aid should therefore be mounted on top of the tower. All required wiring and cabling for the aid should be mounted and secured.

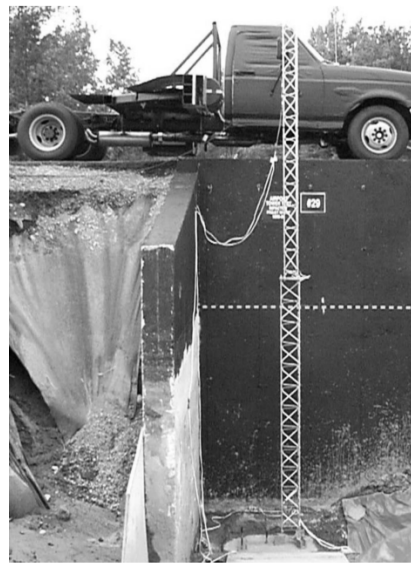
The impactor must be firmly and rigidly attached to the test vehicle to ensure that the interface provided during impact is that of a rigid section. The impact forces should be recorded by load cells

incorporated between the reference impactor and the interface on the vehicle, as close as possible to the mounting location to record the time history and the force of impact. A sufficient number of load cells should be employed to ensure that any moments generated in the impactor due to impacts off its center line are recorded [9]. Impact loads should be accurately recorded from the load cells during the impact test. The ADM recommends using a recording speed of at least 10 kHz to adequately capture the maximum impact forces that occurs within 2 to 5 ms.

The energy over the contact period is calculated by integration of the impact forces with respect to distance. The speed should be accurately and directly recorded from the moving vehicle at the impact time. Due to the extremely short time of impact, typically 100 ms for a frangible mast [9] is physically impossible to visually inspect the failure modes of the mast. High-speed camera or video should therefore be used in order to monitor the impact sequence.



(a) Elevated impactor.[13]



(b) Elevated runway. [9]

Figure 2.1: Typical full-scale dynamical test-setup.

2.2 Acceptance / rejection criteria.

An approach lighting tower should be considered frangible if the maximum impact force recorded during impact are less than 45 [kN] and the impact energy does not exceed of 55 [kJ]. These requirements are related to the structural damage imposed on the aircrafts wing. In the case of an in-flight impact, it is desirable to not significantly impede the flight trajectory. Visual inspection of the failure modes should therefore also be used when determining acceptance or rejection. The major points which influences the frangibility of a mast based on visual inspection are:

- The impacted tower should give way to the passage of the aircraft for a successful landing or continued take-off.
- The portion of the tower above the point of impact should not grasp the aircraft wing while the lower portion of remains "grounded".

- Damaged fragments of the mast from the impact should not cause a secondary hazard to the aircraft (e.g penetration to cabin).

More damage is accepted for ground impacts, and the primary objective for such an incident is to avoid injury or loss of life [9].

2.3 Reference impactors

As mentioned in the introduction, two types of impactors has been used in the development of the ICAO frangibility requirements: rigid and soft impactors. In this section I will present the different impactors and discuss the various challenges in the use of these. Emphasis will be made on the soft impactors as they are the basis for this project.

2.3.1 Rigid impactor

The ICAO Aerodrome design manual (ADM) Part 6 [9], recommends to use a so called “rigid” impactor for dynamic testing of approach lighting structures. The ADM specifies the rigid impactor to be of a semicircular steel tube with an outer diameter of approximately 250 mm. The wall thickness should be sufficiently thick as to represent a rigid body, but no less than 25 mm. The width of the impactor should be 1000 mm or five times the maximum cross-sectional dimension of the tower, whichever is the greatest. A support structure enabling a firm and rigid attachment to the test vehicle should be provided to ensure that the interface during impact is that of a rigid section. The ADM does not specifically define how this interface design and construction is done, but a typical setup which was used in a test-program by the National Research Council for Exel Composites [1] is shown in figure 2.2.



Figure 2.2: Rigid impactor. Photo: M.J Nesad [1].

The use of a rigid impactor as opposed to a more realistic soft wing impactor is based on the results from test campaigns [14] and [15] performed by D.G Zimcik and A.Selmane. The results showed that a more rigid impactor would lead to higher peak forces and shorter contact period than the soft, but hardly any effect on the impact energy and mode of failure (of the mast) [7]. A rigid impactor does not allow for the evaluation of frangibility based on the damage of the impactor. However, there are several advantages with using a rigid impactor:

1. Conservative data are obtained during full-scale, high-speed impact testing.
2. Low production cost, does not require the complex wing section construction as the SWI.
3. No precision needed in relation to materials used or fabrication method applied.
4. Reusable without modification for repeated tests (low test cost).

The recommended impactor was therefore the rigid impactor.

There are however several elements which speaks in disfavor of the recommended rigid impactor. Test results recorded in the load cells tend to be dominated by noise due to resonance problems as presented by Griffith [16], Rølvåg [17] and Dan Duke [12]. Griffith recommended to use a soft impactor in future tests. Furthermore, simulations done by Rølvåg [17] indicates that the rigid impactor generates initial reaction forces far above the ICAO limits when hitting a typical aluminum aviation mast. The rigid impactor also seems to alter the failure mode of support structures consisting of hollow fiberglass/polymer tubes from a global failure to a localized failure. The rigid impactors may slice through such poles, while soft impactors would not, as presented by [12]. This could indicate that the results obtained from test performed with a rigid impactor might not always be conservative [7].

2.3.2 Softwing impactor

During the development of the frangibility requirements, several different variants of the soft impactor has been used. The soft wing impactor on which this project is based on, is the soft wing design that was first used in a test campaign carried out by the National Aerospace Laboratory (NLR) [18]. It was designed to be a structurally identical, but aerodynamical simplified representation of the wing section of a Beechcraft Model 80 Queen Air. The Beechcraft Queen Air, shown in figure 2.3, is of similar size to the Piper Navajo (model PA-31-325) which wing section had been used in earlier test programs [11]. The Queen air has an approximate take-off speed of 140 km/h and weighs around 3000 kg. This impactor was later chosen as the standard soft wing impactor in the following test programs [7]. The



Figure 2.3: Beechcraft Model 80 Queen Air

SWI, shown in figure 2.4, consist of four equally spaced main and front supporting ribs, a mainspar that runs across the entire width of the wing section and an outer skin. The thickness and material of the individual components are taken from [13] and given in table 2.2. The individual components and outer skin are all joined together using rivets. The impactor is then bolted onto a square steel support tube with the outer dimension of 200x200 mm. To account for unrealistic failure modes due to the finite width of the wing section as observed in [18], the outer support ribs are stiffened on the outside. The impactor is in total 1000 mm wide (not accounting side supports) and 640 mm deep. The dimensions of the individual components are given in Attachment 3. In the investigation of a frangibility requirement, the pass/fail criterion for the frangibility of a structure was based on the extent of damage imposed to the wing. Skin damage was considered to be acceptable, but the main

front spar, which is part of the load carrying structure of the wing, must not suffer any critical damage. [7].

The manufacturing of the SWI is considered as a tedious and costly task. If access to commercial production facilities with the appropriate machines and tools aren't available, one rely on custom hand made elements. The mainspar, front and main ribs has to be cut into the desired shape from aluminum plates. The cut plates then has to be bent in order to create the flanges onto which the components are joined together with rivets. The front ribs has a curvature which makes the bending even more challenging. Then comes the tedious task of drilling holes for each of the rivets and assembling it together. One could use pop-rivets to speed up the process, but it is still considered as a time-consuming task.

Table 2.1: SWI components and typical material thickness

No.	Part	Material	Thickness [mm]
1	Support tube	Steel	-
2	End Support	Steel	2.0
3	Main rib	Aluminium 2024-T6	1.6
4	Skin	Aluminium 2024-T3	0.8
5	Mainspar	Aluminium 2024-T3	2.0
6	Nose rib	Aluminium 2024-T6	1.6

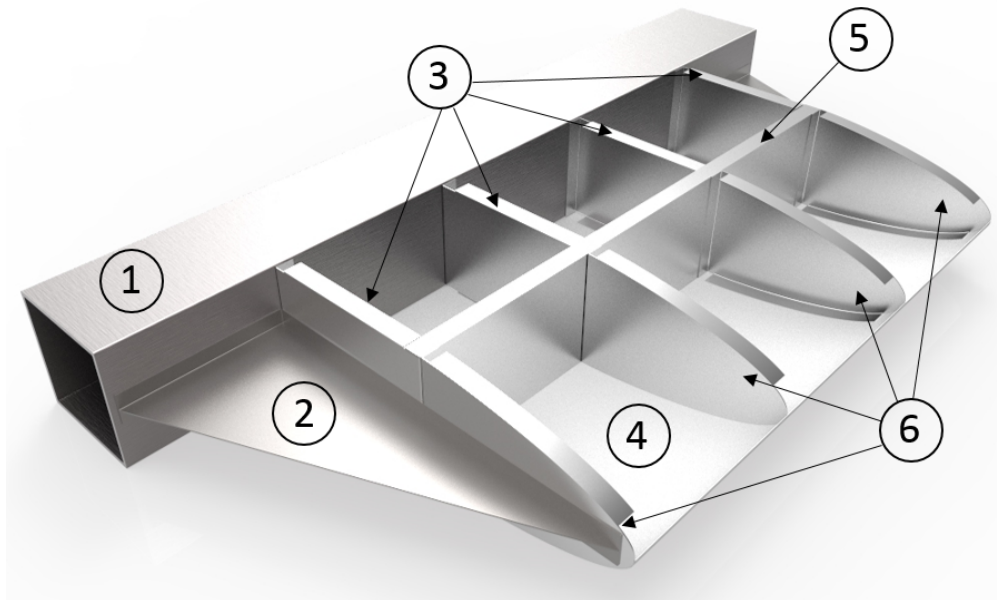


Figure 2.4: Original NLR Soft Wing Impactor

Failure modes

When a new surrogate impactor is to be developed through this project, one relies on static and dynamic compression and impact tests which quantifies the stiffness and strength it should inhibit. The structural properties of the SWI has been rigorously studied through the development of the ICAO frangibility requirements. It is however difficult to analyse the mechanical properties of the SWI based on the full-scale dynamical tests, as these are the result of wing deformation and mast

failure. It is also economically and physically impractical to perform full-scale physical and virtual testing in when developing and benchmarking a proposed solution. Two static compression tests has to this date been conducted, namely by Wiggenraad et. al [2] and Rølvåg [3]. Wiggenraad performed a physical quasi-statical compression test on a non-standard softwing impactor representing the Piper Aztec aircraft used in testing of EXEL ALS [15] as shown in figure 2.5, from now on called a soft-nose impactor. Rølvåg performed virtual compression tests on an impactor nearly identical to the SWI. The results from Rølvåg's simulation which yielded the most reliable deformation modes and accompanying force-levels, and the results from the physical compression test are plotted together in figure 2.6. Rølvåg provided the data's from his analysis and the data from NLR was reproduced from [2] using the Matlab script: GRABIT [19]. The data's are recorded visually from the figure, thus some error are to be expected. These are however considered to be negligible in this respect.

It should be noted that the two mentioned tests are not directly comparable, as neither the test setup nor geometry were completely the same. The intruder, which is the tool in which the impactor is compressed by, that Wiggenraad used had a slightly different cross-section than Rølvåg. Wiggenraad compressed the soft-nose impactor with the intruder centered over one of the middle support rib, whilst Rølvåg compressed the SWI with the intruder centered between the support ribs. They both have a skin thickness of 0.8mm, but the soft-nose is slightly larger in general. The main difference is that the mainspar on the soft-nose impactor is positioned at 450 mm from the nose tip, against 340mm for the SWI. The curvature of the nose on the SWI also seem slightly smaller than the soft-nose. It should also be noted that the deformation modes accompanying recorded forces were not verified at the time this report was written.

Rølvåg defined 7 deformation modes which is reproduced and presented in table 2.2. The first five deformation modes are also observed in the soft-nose impactor. From the test results in figure 2.6 we can see that the SWI is slightly stiffer in deformation mode 1. This might be due to material inequalities, but it might also be because of the soft-nose has a slightly "rounder" front as noted earlier. The second rise of compression force observed in comparable stiffness. This second rise of impact force is related to skin stacking and elasto-plastic deformation of mainspar/mainribs. This occurs at a later stage on the soft-nose solely because of the 100 mm difference in mainspar position from nose tip. The characteristic compression response in figure 2.6 is the one in which the surrogate impactor should mimic.

It should be noted that the two mentioned tests are not directly comparable, as neither the test setup nor geometry were completely the same. The intruder, which is the tool used to compress the impactor, that Wiggenraad used had a slightly different cross-section than Rølvåg. Wiggenraad compressed the soft-nose impactor with the intruder centered over one of the middle support rib, whilst Rølvåg compressed the SWI with the intruder centered between the support ribs. They both have a skin thickness of 0.8mm, but the soft-nose is slightly larger in general. The main difference is that the mainspar on the soft-nose impactor is positioned at 450 mm from the nose tip, against 340mm for the SWI. The curvature of the nose on the SWI also seem slightly smaller than the soft-nose. It should also be noted that the deformation modes accompanying recorded forces were not verified at the time this report was written.

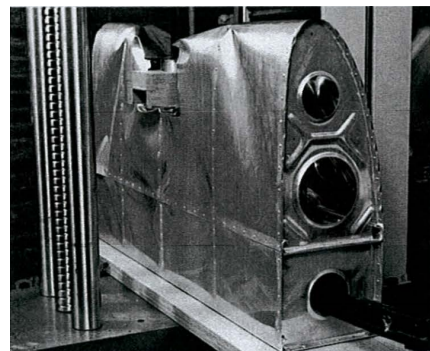


Figure 2.5: Physical compression test. Photo: Wiggenraad [2]

Rølvåg defined 7 deformation modes which is reproduced and presented in table 2.2. The first five deformation modes are also observed in the soft-nose impactor. From the test results in figure 2.6 we can see that the SWI is slightly stiffer in deformation mode 1. This might be due to material inequalities, but it might also be because of the soft-nose has a slightly "rounder" front as noted

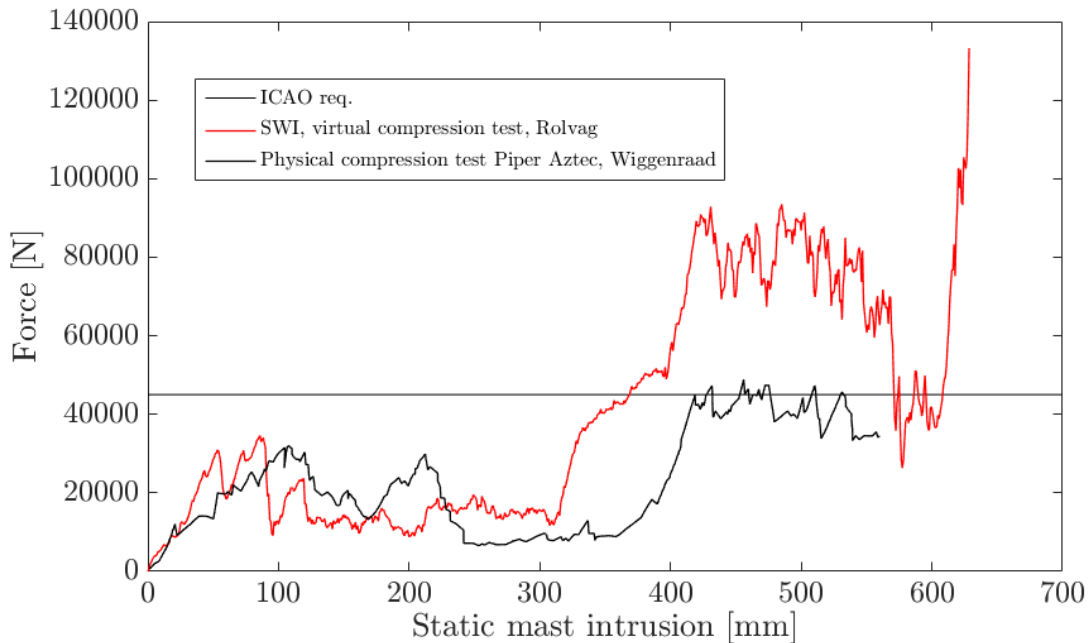


Figure 2.6: Wing impactor compression test results.

earlier. The second rise of compression force observed in comparable stiffness. This second rise of impact force is related to skin stacking and elasto-plastic deformation of mainspar/mainribs. This occurs at a later stage on the soft-nose solely because of the 100 mm difference in mainspar position from nose tip. The characteristic compression response in figure 2.6 is the one in which the surrogate impactor should mimic. The surrogate impactor are to be used in high-speed impact testing of frangible aviation masts, and so the effect of inertia should be taken into consideration when designing the surrogate impactor. Rølvåg [3] also performed a dynamical compression test at the specified ICAO test speed of 140 km/h. Rølvåg reported that the first three deformation modes were altered, and the resulting crush characteristic was altered to an oscillating force at around 20 kN as shown in figure 2.6.

As mentioned earlier, the ADM [9] specifically states that the structural damage on an aircraft during impact is, amongst other, related to the contact area between the aircraft and the impacted object. A small impact area concentrates the impact forces, leading to lower forces to cause failure and vice versa. This is also shown to be the case for the SWI from NLR's compression tests 2 and 3 [2]. This sensitivity to impact area is an important feature which is completely eliminated with the use of a rigid impactor, and also one which the surrogate impactor must inhibit.

Table 2.2: Soft wing deformation modes. Reproduced from [3]

Mode no.	Deformation Mode description	Mast Intrusion [mm]	Force Range [kN]	Energy range [kJ]
1	Linear elastic deformation of skin and main spar.	0-80	0-34	0.0-2.0
2	Skin failure (tear open), plastic shear deformation mode.	80-120	34-13	2.0-3.0
3	Skin in plastic shear deformation mode, constant force.	120-315	13-13	3.0-5.0
4	Skin in plastic shear, stacking up against main spar.	315-420	13-80	5.0-9.0
5	Plastic deformation of main spar and buckling of supporting ribs. Side supports start to deform.	420-540	80-80	9.0-20.0
6	Rib buckling failure, main spar detach from ribs and skin. End supports are stretched inwards	540-590	80-40	20.0-23.0
7	Skin is stacking up against stiff support tube	590-620	40-130	23.0-25

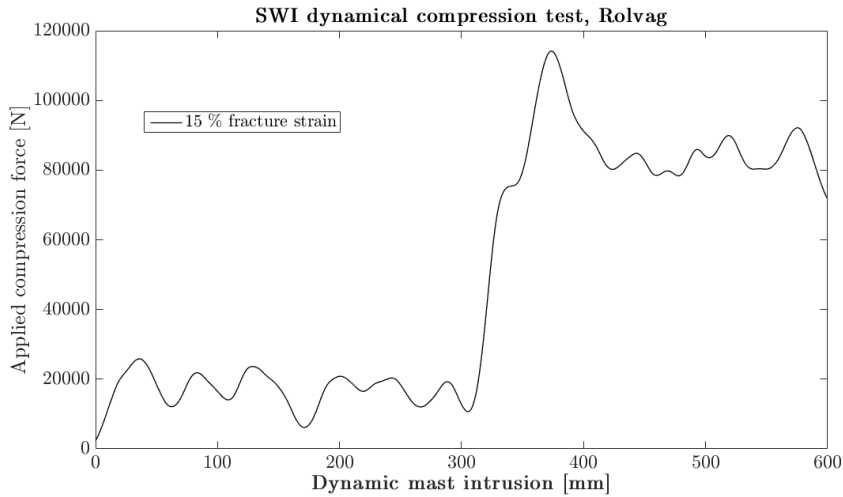


Figure 2.7: Dynamic compression test from [3]

Chapter 3

Design requirements

In product development it is important to identify the requirements that determine the solution and embodiment. These requirements must be formulated and documented as quantitatively as possible [20]. The requirements can be divided into two different categories: User needs and wishes and product performance requirements (kilde). As the surrogate impactor this paper aims to develop is supposed to be used as a low quantity test tool, the main focus will be on product performance.

The design requirements are based on the investigation and analysis of the SWI done in the previous chapters. The result of this chapter will be a set of general design limitations and requirements in which the concepts and ultimately the final solution will be evaluated against.

3.1 User

Since the main focus of this thesis is the structural properties of the surrogate impactor, no user demands has been investigated. It is however of interest to briefly define and describe the users and interested parties of the product as it has great influence on the layout and design of the product.

The typical user of this product (today) are engineers or research scientists with comprehensive knowledge of mechanical testing and production. Typically the testing of frangible aviation masts that has been done to this date, has been outsourced by either the mast producers or governments to institutions like the NLR and universities.

Other parties that has interest in the product are:

- Mechanical workshops whom the task of producing the product is given.
- Frangible aviation mast manufacturers.
- Governments.

For the mechanical workshops, it is important that the new product is easy to manufacture with readily available production techniques. The structure should be easily understood and with well a defined structure. For the mast manufacturers, it is important that the new product is substantially cheaper than the current SWI. As they are responsible of proving their products frangibility, the funding of a crash test would most probably be provided by them. The government, meaning the organization with the primary responsibility of safety and regulations of civil and military aviation, such as the FAA, would be interested in a product with high accuracy and reliability.

It is assumed that the user of the product has basic knowledge and skills to mechanical assembly/construction.

3.2 Product requirement

3.2.1 Structural properties

The purpose of surrogate impactor is that it realistically and as accurately as possible, represent the structural stiffness and strength as an actual aircraft wing. Ideally these properties should be collected from a full-scale wing-structure. Since such a study is impractically and economically difficult to conduct and since no such tests has ever been conducted to my knowledge, the SWI used in the development of the ICAO frangibility requirements shall be used as a reference for the design loads. The new impactor should therefore mimic the crush characteristic as shown in figure 2.6 and further described in table2.2

Energy requirements

In the development of ICAO frangibility requirements, the speed during impact was considered as constant. This lead to the force-deflection curves instead of force over time. The energy is calculated from the integral of energy over static mast intrusion ($N \cdot m$). Energy imposed is therefore only dependent on the force-deflection, and hence if this matches, energy will too. No emphasis will therefore be .

Torsional stiffness

The new product should provide torsional stiffnes, as to prevent any undesired bending upon impact, as observed for the SWI.

3.2.2 Cost

The cost of the SWI was estimated to be approximately 4000 - 5000 NOK/impactor in raw-material alone (see appendix X). The most expensive component was the main support tube, which contributed to almost 1/4 of the total estimate. This is because the price of the main support includes the cost related to production. The labor cost of producing the SWI, which is considered as the largest contributing factor in the total cost, was not accounted for in this estimate. This is because it is difficult to estimate the time it takes to manufacture and assemble the individual components. The estimate does account for some loss of material related to the production process, but was optimized as far as possible, and some additional loss should be accounted for. Nor was the costs related to transportation accounted for.

The market for this product is in the low range. The total number of impact tests which has contributed to the frangibility requirements is 52, whereas 36 of these were done with either a standard or non-standard softwing impactor [7]. Since 2000, only two crash tests has been reported [1] and [16], to the authors knowledge. So it is difficult to quantify the cost target value. As a minimum requirement, the solution should not cost more than the SWI in raw material, e.g. it should cost less than 4000 NOK/impactor.

3.2.3 Geometry

As the product must comply with the ICAO standards given by the ADM [9], the new product must be 1000 mm wide, and should be scalable. Since it should simulate the impact of a wing, it should have roughly the same shape. This means that the overall shape should be no wider than the outer dimensions of the rigid impactor of 250 mm, but no smaller than the widest part of the SWI of 200 mm. No limitations has been set for the depth of the impactor, but it should be within reasonable limits to properly handle and mount the impactor on the vehicle.

On appearance: Since this is a tool intended for crash tests, less to none focus should be on the products appearance. A product in a similar shape as an actual aircraft wing is to be preferred.

3.2.4 Insensitive to eccentric loading

Studies of photographs from earlier test programs such as [21] and [13] shows that the impact position on the impactor is difficult to easily precisely control when driving at a speed of 140 km/h. In several of the test, the mast hit close to the outer rib. It would be easier to control the point of impact with a guided rail-wagon. However, the current standards opens up to the use of a truck-mounted impactor. The new impactor should therefore be insensitive to a non-centered impact.

3.2.5 Load cells

The current standard requires the peak load upon impact to be recorded and documented. In order to reduce the cost, it would be favorably to avoid the expensive load cells (assumption) and sophisticated interface between impactor-load cells-support structure. One could design an impactor that the frangibility requirement is determined entirely on visual inspection. However, as the standard is to this date, load cell should be incorporated in the design.

Chapter 4

Concept development

Now that the product performance and some general design requirements for the surrogate impactor have been identified, the next phase of the project is the concept development. In order to generate concept in the most effective way a structured approach, a structured approach to the problem reduces the likelihood of costly and time-consuming problems. In addition, a structured approach to concept generation opens up the “solution-space” and facilitates something clever. In this project, a five-step concept generation method described by [4] has been employed. This method is a commonly used method at the institute of which this project is written at. The five steps are outlined in figure 4.1 which is reproduced from [4]. The method breaks a complex problem into simpler sub-problems onto which solution concepts can be identified by external and internal search procedures. Classification trees and concept combination tables are then used to systematically explore the space of solution concepts and to integrate the sub-problem solutions into a total solution [4].

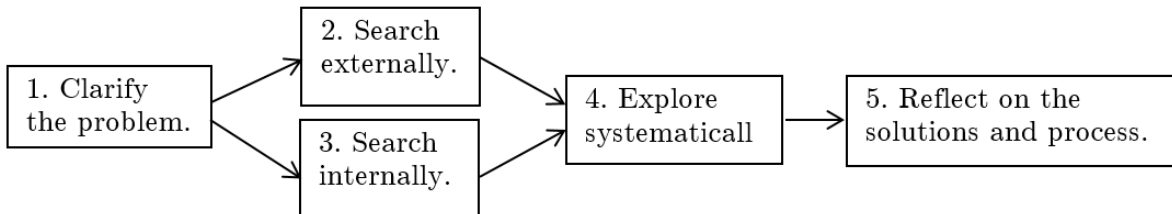


Figure 4.1: Five - step concept generation. Reproduced from [4]

In the following a brief description of the results from these steps are presented, and summed up in a classification schemes. The most promising solutions are outlined and presented.

4.1 Problem decomposition

The first step of clarifying the problem has at some degree already been investigated and documented through the description and analysis of the rigid and soft-wing impactor. From the deformation modes of the SWI in table 2.2 with the corresponding force and displacement range, we can idealized the crush-response that the new impactor should inhibit for simplicity. The design curve in figure 4.2 will serve as an overall design paramater for the dynamical properties in which to design after. As shown in figure 4.2, the SWI has five deformation modes which are thoroughly described in the previous chapters.

Deformation mode 5 is related to mainspar damage, and hence frangibility requirements is ment. In fact the requirements are exceeded before mainspar collapse. The surrogate impactor should therefore inhibit the characteristic crush-response 1-4 in figure 4.2 The strategy in this conceptual phase is to

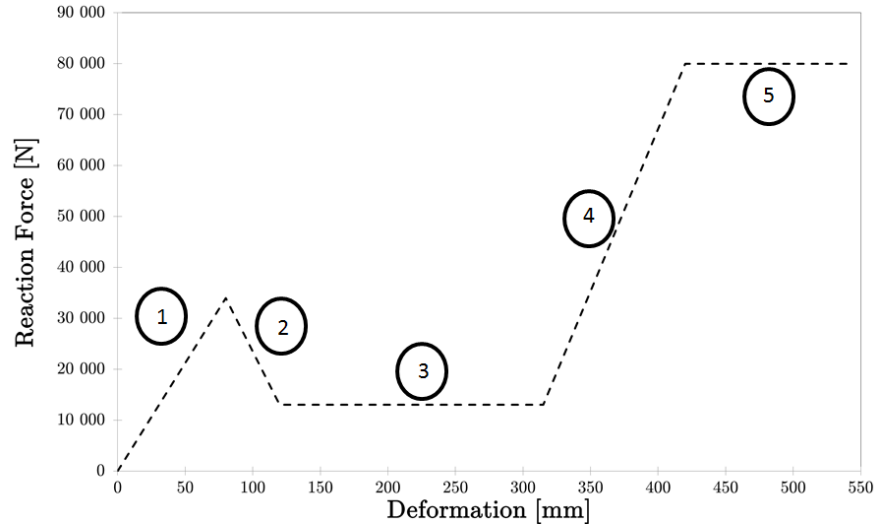


Figure 4.2: Idealized compression response

divide the first fire deformation mode, and investigate them individually. The total response could then be to combine these findings into the total reaction curve. In order to produce the crush-characteristics of the SWI, three different functions were defined:

1. Linear-elastic.
2. Failure.
3. Constant force.

A combination of these three works as a basis, and was then investigated separately through step two and three.

4.2 Search externally and internally

The external search is aimed at finding existing solutions to both the overall problem and the subproblems defined in the previous chapter. By using a broad-search and investigate sources like patents, commercial products and published literature one can find solutions to the individual subproblems. In this project, this step is confined to searching for existing products and published literature, as the users of this product was not easily contacted. In the following, a brief presentation of the findings that was done in the project initial phases is performed. A brief description of the most useful findings are presented, and summarized in a classification scheme. The internal search consisted of analysing what failure modes produced the individual crush response. They are presented together as the findings were limited.

4.2.1 Subfunction 1: linear elastic

- Springs exerts a linearly increasing force by deformation ($F=kx$). They are predictable but may be of high cost due to combination of high stiffness and large deformations.
- Beams which is suspended at both end and which are free to deform in the middle produce a linearly increasing force when deformed. Metal beams with simple cross-section could also apply subfunction 2 as it would fail at a certain level.
- U-shaped metal beams and tube which is unsupported produce a linearly increasing force by deformation because of its round shape and elastic properties.
- The elliptical skin in the SWI are known to produce the desired deformation mode 1-3.

4.2.2 Subfunction 2: failure

Not much was found here, but beams which is constrained in such a way that they buckle could produce the failure and successive loss of material strength.

Failure in the material, such as shearing of rivets, shearing of skin and such could be utilized. Introducing failure elements in the material such as notches creates stress raisers which enhances failure.

Fuse bolts is a bolt which has grooves machined in the center of it. It breaks at a certain load level due to the stress raisers induced. This could be used in combination with for example springs to produce the initial two deformation modes.

4.2.3 Subfunction 3: constant force

The constant force related to skin shearing and buckling of skin on the SWI has been observed to yield constant forces.

The most important findings in this study was however that honeycomb structures, which are commonly used in energy absorption systems as they, when loaded axially beyond its ultimate compressive peak strength, will absorb energy at constant stress [5]. The crush characteristic is shown in figure 4.3 b). The honeycomb can also apply to subfunctions 2-3, or it can be precrushed to apply only to subfunction 3. Can be of both aluminium and composite and the mechanical properties is fairly predictable. They are typically high in price range (99.4 - 166 NOK/kg), but this may be cancelled out in the sense that production is outsourced and its readily available.

Foams also possess the property of asserting constant stress during axial crushing. Difference is they do not exert a peak load higher than crush load, meaning that when failure occurs, the stress is held constant. Comes in a range of materials like ceramic, polymers and aluminium. One advantage of using foams is that they are considered as an isotropic material, meaning that they have the same mechanical properties in all three directions.

This concludes the findings that was done. It became imminent quite early that this method was in fact quite ineffective, and so emphasis was made on concept generation and testing. The findings that were done was ordered in a classification scheme however, and served as a tool in producing solutions which might not have been thought of earlier.

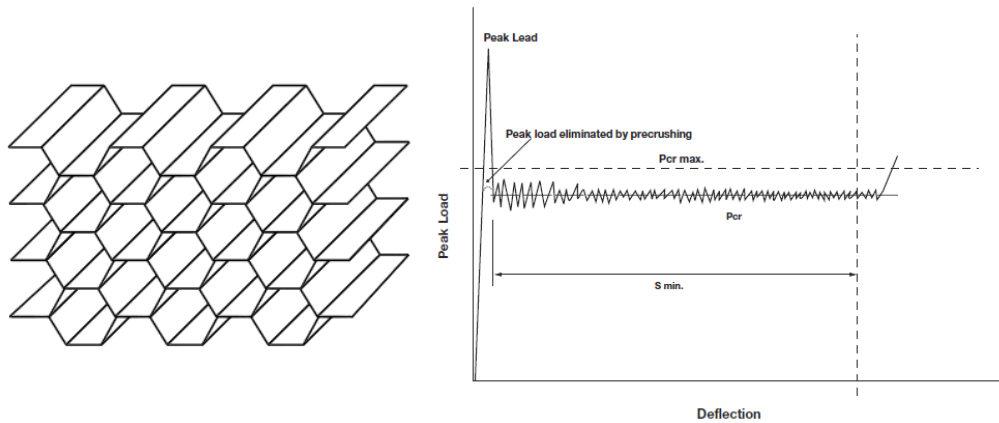


Figure 4.3: Hexagonal Honeycomb with typical crush characteristics (from [5]).

4.3 Classification scheme

Table 4.1 shows the individual findings for the subfunctions which was done. It is arranged such as the deformation modes are listed vertically, and horizontally the solutions for the deformation modes are placed. Some are stretched over multiple deformation modes, this means they may produce all the deformation modes it produces. Outlined are the four most promising concepts which has been investigated in this project. In the following sections, a presentation, testing and evaluation of the different concepts are presented.

Table 4.1: Morphology table

1				
2				
3				
4				
5				
5				

4.4 Concept A

If we compare the quasi-static compression test simulations done by Rølvåg [3] and the compression test done by NLR [2], the mechanical properties are a fairly good match despite their differences. NLR used an impactor which represented the mast used in a test-programme performed by the NLR for Transport Canada [15]. Rølvåg used a square intruder representing the Lattix aluminum light towers, onto which impact tests were performed by Sentek/Agder College [21]. The impact area of the intruders were approximately the same (NLR intruder about 2.5% larger), but their cross-section differ. In Rølvåg's simulation the intruder was positioned between the two middle support ribs. This is where the impactor struck the towers in the dynamical tests. It is also at this position that the structural strength was assumed weakest. In the NLR compression test intruder was centered over one of the middle support ribs. These results could indicate that there is no major difference in mechanical properties between the impact positions, and hence the SWI could be insensitive to eccentric impact. Concept B is inspired by this fact.

The concept principal structure and boundary condition are shown in figure 4.4. It is basically a

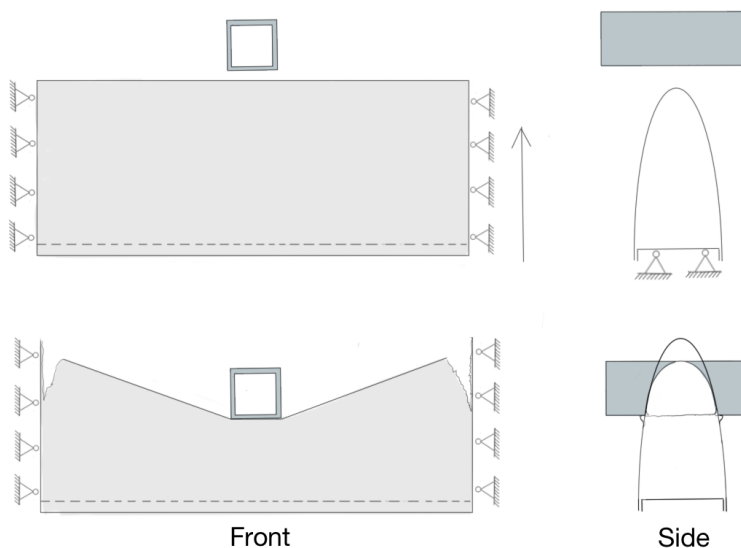


Figure 4.4: Concept A

simplification of the SWI, where the two center support columns consisting of the nose- and main ribs are removed. A "rigid" support structure at each end is instead provided to facilitate reuse. The thesis behind this concept is that by increasing the skin thickness, the loss of structural stiffness by removal of inner support-structure is somewhat regained.

In this concept the only part that is replaced during testing is the outer skin and mainspar, if damaged. This in turn reduces the material use, and thus test costs.

By removing the complex structural components; nose and main ribs, we drastically reduce the production costs of the impactor. In addition to reduced material consumption, you eliminate one of the most complex production methods; forming of the nose-ribs. This process requires special forming tool in order to be performed as if it was an actual wing design. The assembly time is considered to be drastically reduced, as the drilling and riveting is one of the most time consuming processes.

This concept is therefore more a simplification of the original SWI. The concept is illustrated in figure X and consist of the outer skin of 0.8 mm which is structurally locked on each side with a clinching device. The idea is that the outer skin is the only component that is replaced for each test. Instead

of replacing the entire softwing with its structural components, you would only have to replace the outer skin which is, if designed properly, less time-consuming and material efficient.

At this stage, parameters such as skin materials, geometry and boundary conditions feasibility is not considered. These are parameters which is supposed to have great effect on the products structural integrity, and should be further evaluated if chosen. The geometry, and material was chosen to be similar to the SWI at an initial conceptual phase because it is likely to inhibit the desired structural response. Therefore there will, in theory, exist at least one solution to the concept.

Advantages:

- Reduced material consumption.
- Reduced production time.
- In conformity with the current product.
- Semi-reusable.

Disadvantages:

- May be sensitive to eccentric loading.
- High lead time between tests.

4.5 Concept B

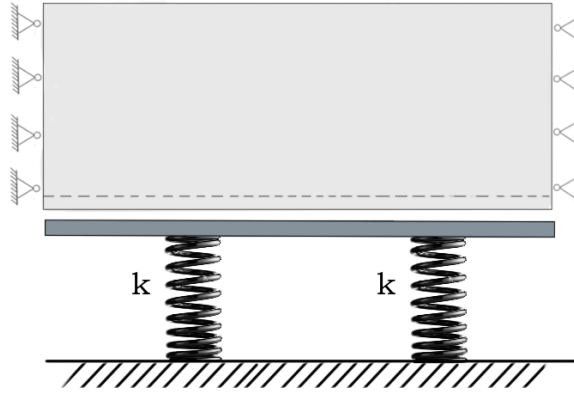


Figure 4.5: Concept B principle structure.

Concept B consists of an aluminum outer skin, like the one in concept A, but instead of a beam as mainspar, springs are placed behind the skin to represent the deformation of mainspar and buckling of main ribs. By removing the mainspar we reduce the number of elements that must be interchanged between impact tests. The concept's principle structure is shown in figure 4.5.

The springs are connected to a steel plate which acts as the physical representation of the mainspar, whilst the springs represent the mechanical stiffness of the mainspar. The assumed deformation mode and corresponding forces are as follows:

1. Skin deforms linear elastic to a designed peak force of about 34 kN
2. Skin tearing and buckling/failure, decreasingly force.
3. Skin in plastic shear deformation, stabilized at 13 kN
4. Steel plate connected to spring is hit, linearly increasing reaction forces.

The assumed load vs static mast intrusion is shown in figure 4.6. The plot shows the assumed reaction force from the skin (green), the spring (blue) and total forces recorded in load cells (red). The plot also illustrates a possible design challenge with this setup; the plate connected to the springs has to be positioned at a distance h from the ends of the skin. If not we get a sudden loss of strength when the skin is totally sheared and failure occurs. This is although easily resolved by making the skin extend sufficiently past the position of the plate. Furthermore, this feature can be utilized to evaluate if the ICAO force-requirement are exceeded. This would eliminate the need for expensive load cells and the post-processing of test data. It may be however that when inertia and damping forces are introduced in a dynamical impact that the solution becomes not that predictable.

The stiffness k of the springs is easily calculated from the “linear” rise of reaction force related to mainspar deformation. The springs exert a linearly increasing force $F = kx$ where x is deformation. By measuring two sets of data (Force,displacement) and use the relation $K = (F2 - F1)/(x2 - x1)$ we can calculate an approximate value of spring stiffness. The two data points can be taken from the force range vs. deformation range of deformation mode 5 in table 2.2. The total stiffness of the two springs in total would then be $K = 638$ [N/mm]. Springs connected in parallel has a total stiffness of $K = k1 + k2$ [22]. Since the two springs must have the same stiffness, we get a stiffness of $k = K/2 = 319$ [N/mm] for each spring. This is a relatively high stiffness, and stock springs with equivalent stiffness can be bought from a vendor. The challenge is rather to find a spring which both has high stiffness and facilitates large displacement. That being said, the spring configuration in figure 4.5 and

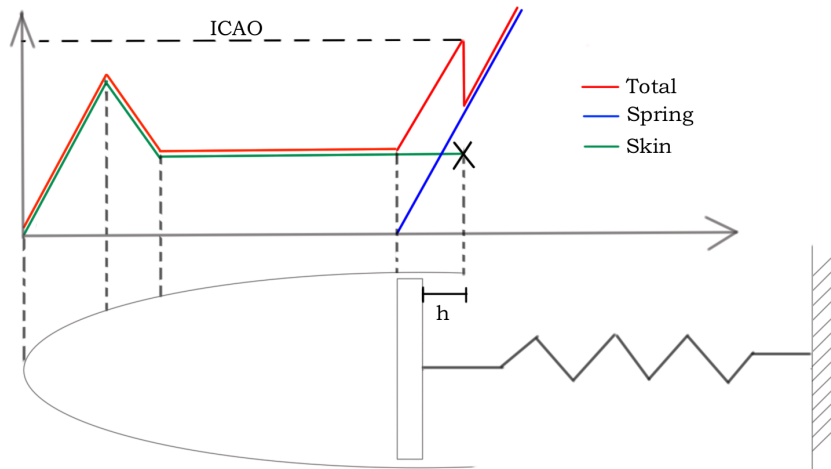


Figure 4.6: Assumed force-deflection Concept B.

the corresponding stiffness calculation are only used as an example. A number of different springs and configuration are possible. Both Push and Pull springs could be used, such as helical springs which are both push and pull. It may be that a push-spring configuration would facilitate the combination of large deformations and stiffness better. This would have to be further considered should this concept be chosen.

It is desirable to increase the number of springs in order to get as evenly distributed forces over the plate width. Full scale dynamical impact test show that it is difficult to hit the wing impactor in the center, a setup with only two springs would be sensitive to eccentric loading, whilst a setup of 10 springs (although unlikely) is considered less sensitive because of the evenly distributed forces. This could however be controlled by adding structurally boundary conditions which controls the motion.

The use of springs can be considered as both an advantage and as a dis-advantage. With the current standards and test procedures it is considered as a large investment to add springs instead of a single beam for the mainspar. If large amount of tests were to be conducted, this concept is a valuable solution. The main disadvantage of this concept is however that the introduction of a steel plate makes the impactor insensitive to impact area. For example: Two masts hit the plate. Mast 1 has a given surface area of 2 and stiffness K while mast 2 has a surface area of 1 with the same stiffness K . Realistically, mast 2 should penetrate the skin and mainspar with less resistance, giving much lower recorded reaction forces than mast 1. In this concept however, mast 2 would break. In addition, if the force exerted by the mast during impact is lower than the compressed spring forces, the springs would push back onto the impacted mast. However, since the impact duration is 100 ms, this is considered as an unlikely event.

4.6 Concept C

This concept is based on the fact that when we take in account inertial effect in a dynamical compression test, the first three deformation modes are changed. If we treat the force-characteristics measured by Rølvåg [3] in a conservative manner and say that the surrogate impactor should have a sudden impact force up to around 30 kN, followed by a relatively constant force around 20kN until the mainspar is hit, drastically increasing the reaction forces to a force level beyond the ICAO requirement.

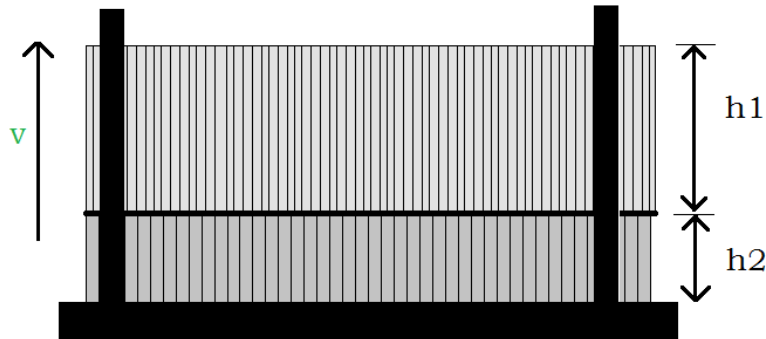


Figure 4.7: Concept D

The concept is shown in figure 4.7 and is basically two honeycombs with different compressive strengths placed on top of each other. This will in theory produce the crush characteristics described. When the first honeycomb is struck, the force will drastically increase to a designed force level. As the honeycomb cell walls start to buckle, it will remain constant at that level until the honeycomb starts to densify and stack against the second honeycomb. What happens then is that the force will rapidly increase to a designed force level until honeycomb 2 starts to buckle. The honeycombs are quite stiff in the linear-elastic region, which produces a much more rapidly increasing impact force than the SWI. This may not be a substantial problem, as the two honeycombs alone would be a much more realistic representation of the SWI than the rigid impactor, but can also be accounted for by adding an aluminum tube or springs. By adding a tube, this could produce the softer characteristic of the SWI, and the honeycomb buckling produces the failure at around 32 kN and the subsequent constant crush load.

The honeycombs compressive strength are assumed to be eliminated or reduced in some matter by the geometrical shape of the object (mast) that it is impacted by.

Another feature with this concept is that it is versatile. One does not necessarily need to use two honeycombs in order to validate if the force requirement is exceeded. If load cells are to be applied in the test, one would only need one honeycomb since the force level is exceeded before mainspar actually fails. A further evaluation of test procedure should be discussed to conclude this, but the possibility is present in this concept.

The main advantage of this concept is that the honeycombs are self-supporting structures. This leads to a very simple setup of the impactor. Also, the individual honeycombs are replaceable. If honeycomb 1 is damaged but honeycomb 2 is still intact, one simply has to replace the top honeycomb, leading to lower test cost. The characteristics of an aluminum honeycomb are fairly predictable and substantial amount of research has been performed on them, as they are commonly used in energy-absorbing systems.

A disadvantage with this concept is that the honeycombs themselves are a fairly complex structure. Leading to a relatively high cost-per weight at 90-160 NOK/kg (kilde). They require the use of

certain production equipment's which means that only certain kinds of businesses at given geographical locations are able to produce them. On the other hand they are in some degree standardized, which leads to fewer uncertainties. There are also several different suppliers of standardized honeycombs, so one can ideally order one from their production facilities and have them shipped to test location. This can also be controlled by the organization in order to ensure reliable results.

The main disadvantage of using honeycombs to replicate the crush-characteristics of the SWI is that honeycombs are considered as an orthotropic material. This means that they only inhibit the described crush characteristic in one direction. The honeycombs are therefore quite sensitive to impact loads with an impact angle only a few degrees off its center axis. This is undesirable in physical high-velocity impact tests of frangible aviation masts, as the contact direction upon impact is altered when the mast starts to fail and deform. Furthermore, dynamical crushing of honeycomb samples having heights that are considerably greater than their width leads to lateral collapsing of honeycomb stacks, as reported by F.Doengi et al.[23]. These effects can however be accounted for by installing some sort of lateral guiding system. The black vertical lines in figure 4.7 are indication of two tubes on each side of a support tube, which was provided to hold the honeycombs in place. These will provide some transverse stiffening, but this is decreasingly towards the centerline of the honeycombs. Two variants of a lateral guiding system for controlling the axial crushing of the aluminum honeycombs has therefore been investigated in this conceptual phase.

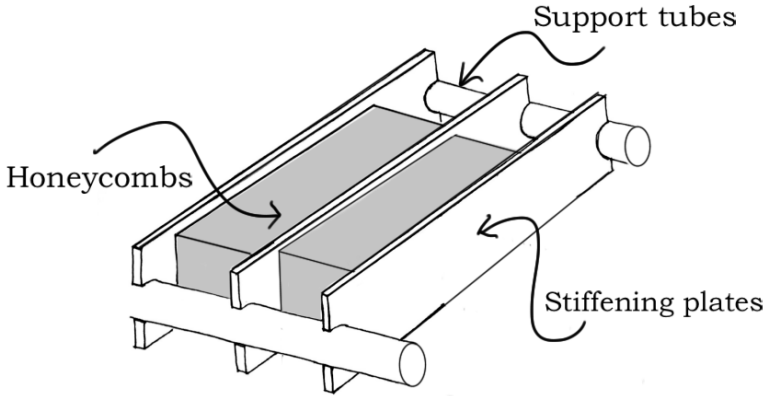


Figure 4.8: Lateral stiffening 1.

The first version of lateral stiffening, shown in figure 4.8 is a guidance system which is similar to the surrogate test vehicle (bogie), which are used by the US Federal Highway Administration (FHWA) to reduce the test costs related to full-scale crash testing of highway appurtenances [24]. The bogie utilizes honeycombs to mimic the crush characteristics of a small size vehicle. In this setup, two tubes positioned at each end of the honeycombs provide the lateral stiffness, while plates between the honeycombs connects and constrain the honeycombs to the support tubes. The plates are allowed to slide along the tubes length, but are constrained in the lateral direction by semicircular holes at each end. This ensures that the honeycombs are crushed axially, and thus the system becomes quite predictable and the results are repeatable/comparable.

Advantages:

- Easily replaced honeycombs between tests.
- High lateral stiffness.
- Already tested and utilized product.

Disadvantages:

- Insensitive to mast impact area.
- Added structural elements and weight may change the dynamical response by adding/removing inertia effects.

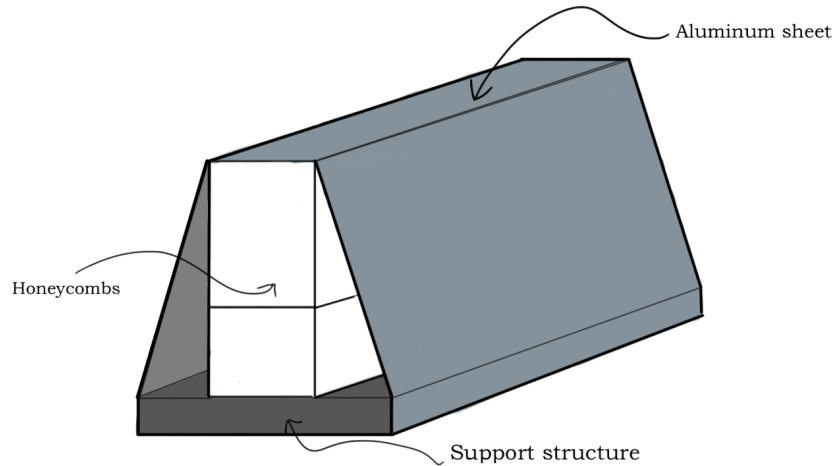


Figure 4.9: Lateral stiffening 2.

The second version of providing lateral stiffness is shown in figure 4.9. A thin aluminum sheet has been added on the outside of both honeycombs. The sheet is bent over the honeycombs and joined to each side using a strong adhesive, such as the ones used to join the individual cell walls of the honeycomb. The aluminum is then bolted or riveted to the support beam for added support. The idea is that the aluminum sheet will stabilize the honeycombs outer cell walls and prevent lateral buckling.

Advantages:

- Self-supporting.
- Small changes in weight/volume leads to small inertial effects.
- Sensitive to mast impact area.

Disadvantages:

- Added material cost.
- Less lateral stiffness than version 1.
- Each test requires two honeycombs.

4.7 Concept D

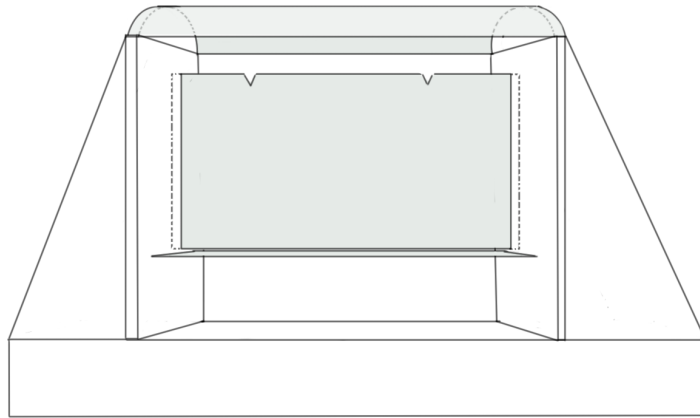


Figure 4.10: Concept D

This concept, shown in figure 4.10, is a result of superposing the individual failure modes, treating them as individual components. It is composed of a front beam with a semi-circular cross-section, one or two plates and a back beam. The concept rely on using simple beams and plates which are easily replaced. This allows us to construct a single support structure which then are utilized in every tests. By using beams and plates should in theory the number of insecurities related to production (such as rivets), if support structure is of simple but robust design.

Only the damaged plate(s) and beams would be replaced, based on the degree of damage imposed during tests. It is however reasonable to assume that the front beam and shear-plate(s) must be changed in every test. It is therefore of great importance to focus on the assembly/dis-assembly of these components. The idea behind this concept is that each individual component represent one deformation mode defined in 2.2.

The deformation sequence of concept G is illustrated in figure 4.11. Upon impact with an object, the front beam starts to deform elastically until plastic failure and tearing occur. The front beam is most likely to fail at the left and/or right attachment point, as indicated by red lines. If front beam failure occurs, the mast then proceeds to hit the plate(s), which in turn buckles and ultimately deforms in plastic shear. Notches has been introduced in the plate for two reasons: easily predict the failure point and ensure shear deformation occurs. The notches act as stress intensifiers and introduces a defect in the material. This will, in theory, act as a instigator for failure which allows for less complicated load bearings as the bearings would't carry as much load as if the failure happened at the flanges. When the "shearplate" is fully deformed, the deformed skin starts to stack up against the back beam which represent hitting the mainspar on the SWI. Upon a designed load the back beam then fails due to tearing and the force requirement is exceeded. The back beam can be designed to fail at 45 kN, leading to evaluate if the mast tested is frangible or not based entirely on visual inspeapection. Or, it could be designed to fail at loads onto which the mainspar in SWI

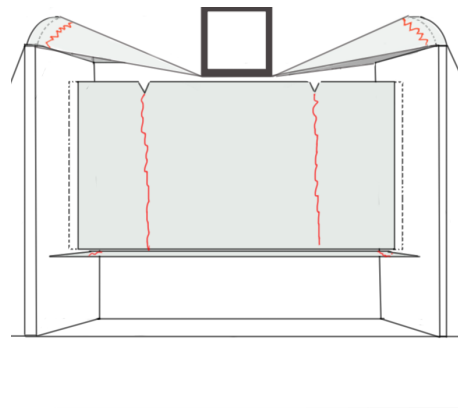


Figure 4.11: Failure sequence.

actually fails, which would require the use of load cells in order to confidently determine pass/fail.

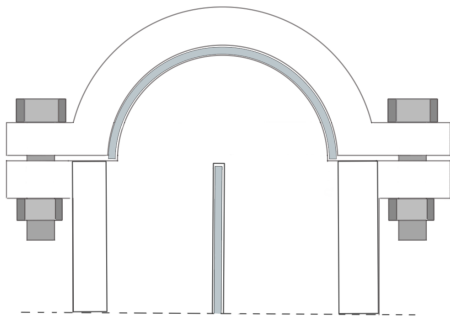


Figure 4.12: Front beam fixture concept

The front beam could be mounted to the support structure by using rivets, bolts or some sort of clamping device (or a combination) as shown in figure 4.12. The figure shows the support structure, a locking flange and bolts. As the bolts are fastened, this will introduce a pressure over the front beam skin. The frictional forces introduced should be sufficient to fix the front beam. This would have to be further investigated if this concept is to be chosen. The beam would possibly have to be pre-formed because of its small shape. Since it already has to be processed it could be more efficient to predrill some holes in the skin and fasten the beam with bolts. This would have to be investigated further should this concept be used.

When mounting the plate(s) representing the skin shear failure mode, they are supposed to easily slide into slots/grooves in the support structure. Figure 4.13 shows two different methods to fix the plate(s). In mounting 1, the plates are slid into the slot and then bent 90 degrees inwards onto the support structure after inserting the plates into the slots. The arrows indicate the bolts/rivets which fastens the plate(s) to the support structure. In mounting 2, the plate is simply slid into the slot and bolted or clamped onto the support structure also indicated by arrows. The two mountings both have its advantages and disadvantages. Mounting 1 reduces/eliminates the axial forces that the mounts would carry. This allows for smaller dimensions in bolts. The plates would possibly have to be pre-bent, which would increase production time. It is possible to bend the plates during assembly, but this might not yield adequate results. Mounting 2 is extremely simple and does not require any processing of the plate(s), but requires higher compression forces by bolts or clamping device as the only counter-force is the one introduced by frictional forces between bolts, plate(s) and support structure.

The back beams could be fastened using one of the same principles as the plates. Because of the high axial forces in the back beam a solution as the one in figure 4.13a would probably be a better solution. This would have to be further investigated if this concept is to be chosen. A negative fea-

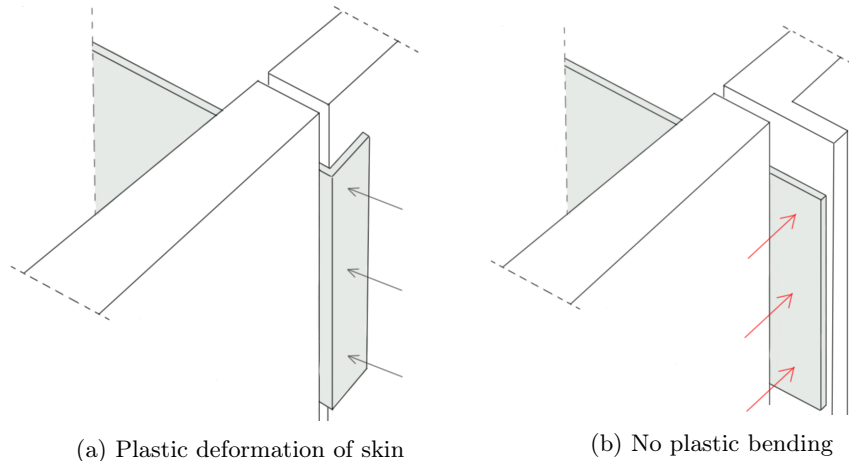


Figure 4.13: Shearplate fixing

ture with this concept is that it may be a tedious task to replace the plates, leading to higher lead times.

4.8 Proof of concept

The purpose of this section is to get a further basis for the concept evaluation and elimination. The embodiment of a concept can be a tedious task, and by prescreening the concept at a principle stage, one reduces the risk of investing time on concepts whom which does not inhibit the desired properties. Furthermore, the mechanical response and stiffness of impact are not easily calculated. In order to evaluate the structural integrity of the concepts it was therefore at an early stage decided to perform FE-simulation on extremely simplified models based on the principle structure described. Typically FE-simulation and analysis are introduced at a much later stage in the product development process. As the ultimate purpose of the surrogate impactor is to mimic the mechanical properties of the SWI, the simulations were performed to get a better basis for decision making. The test was done in as close relation to the ones performed by Rølvåg et.al [3] and Wiggenraad [2]. The simplifications of the models were based on two assumptions:

1. The boundary conditions described are feasible.
2. The support structure of the individual concept is considered to be rigid relative to the material on which is impacted.

These assumptions allow us to exclude any complex support structure and mountings in the FE-model. This drastically reduces the simulation time, allowing for several alterations/iterations to be with respect to geometry and material thickness. All simulations were run in ABAQUS Explicit, using a general contact algorithm enabling all with self-contact and non-linear deformations. The coefficient of friction (μ) was set to 0.2 in these tests.

The concepts which will be investigated at this stage are Concept A, Concept C and Concept D. Concept B will not be investigated on the basis that we can draw some conclusions on the mechanical properties of concept B from the results from Concept A. The only difference between them is how the second rise of impact force is done. It is a fairly good assumption the springs will exhibit the described increase in force vs deflection, at least in a quasi-static analysis. In the following a discussion about material definition, model assembly, geometry and model are presented and finally results are presented.

4.8.1 General test setup

The initial concept verification tests was conducted in as close as possible compliance with the compression tests performed by Wiggenraad [2], as shown in figure 2.5. Wiggenraad used a 250 kN Schenck Trebel static test machine, and placed the soft-nose impactor on a plywood plate in order to fix the lower part of the impactor and because of the finite width of the bench. These conclusions are based entirely on visual inspection of the test photographs that came with the report 2.5. An attempt was made on documenting the setup of the compression test bench with regards to force-measurement with no luck, but the assumption was made that it was performed as a uniaxial compression test, meaning that the forces in the transverse direction are not recorded.

The general simulation test setup and boundary conditions are shown in figure 4.14. The setup consists of two fixed reference points, which acts as the imagined connection to a vehicle support-frame. The reference point also acts as the load-cells in which reaction forces can be registered from. To simulate a support

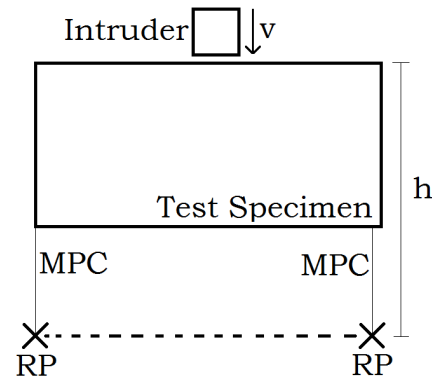


Figure 4.14: General test setup.

structure, the individual concept's principle structure was connected to the reference points using multi-point constraints (MPC's). The connection points/facets to the test specimen are further described in the individual concept description. This same setup was used in all the compression tests, with different attachment points to the concept principal structure, which will be further described under the individual concept analysis.

The two reference points were positioned at a distance h of 840 mm from the initial contact position, and aligned with the impactors proposed mount position. 840 mm is the distance from the load cells and the nose-tip of the SWI. It is strictly not necessary to do this; any arbitrary position connected through the MPC's would completely fix the skin. It was however done, as close as possible, to get comparable results to the earlier compression tests and to record any moment generated. The reaction forces was taken as the sum of the reaction forces in the y -direction (axial).

The intruder, which is the object of which the concept impactor are compressed with, is exactly the same as Rølvag [3] used. It was modeled as a square tube with the outer dimensions of 197.5 x 197.5 mm. To eliminate any intruder deformation as reported by [3], it was defined as a rigid body. The intruder was centered above the every test specimen as shown in figure 4.14, and the quasi-static compression test was performed by giving the intruder a constant velocity of 50 mm/min which is also the same as in earlier tests.

4.8.2 Material modeling

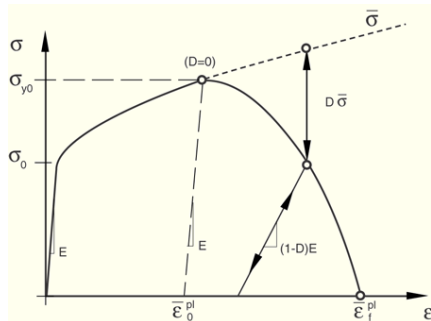


Figure 4.15: Typical stress-strain diagram for a ductile material.(from [6])

and displacement are plotted in a stress-strain diagram. A typical stress-strain diagram of a ductile material is shown in figure 4.15. The stress-strain diagram consists of an elastic and inelastic portion. The elastic portion (a) of the stress-strain diagram corresponds to the stress and strains at which the material, upon unloading, returns to its original state. The inelastic portion (b) of the stress-strain curve corresponds to the plastic deformation (yielding) of the material, meaning the material suffers irreversible damage and rearrangement of interatomic bonds, e.g. does not return to its original state.

A material model is a mathematical relation which describes the stress-strain curve. There exist several different material models, each able to describe a material deformation during axial tension in varying degrees of accuracy depending on the nature of the stress-strain curve. Examples of such material models are elastic linear-hardening, elastic power-hardening and the Ramberg-Osgood Relationship [25]. In this conceptual phase the elastic linear-hardening relationship, from now on referred to as the

bi-linear material model was chosen. The bi-linear material model are described as follows:

$$\sigma = \begin{cases} E\varepsilon, & \varepsilon \leq \varepsilon_{0.20} = \frac{\sigma_{0.2}}{E} \\ \sigma_{0.2} + E_t(\varepsilon - \varepsilon_{0.2}), & \varepsilon > \varepsilon_{0.2} = \frac{\sigma_{0.2}}{E} \end{cases} \quad (4.1)$$

Where E is Young’s modulus, E_t is the inelastic tangent modulus, $\sigma_{0.2}$ is the 0.2% proof stress commonly used for estimating yield stress in ductile material without a clearly defined yield point. The bi-linear model is one of the simplest model of the three, and are useful as a rough approximation for stress-strain curves that rise appreciably following yielding [25]. The bi-linear model was chosen on this basis to obtain conservative estimates of the crush-characteristics of the test specimens. The bi-linear plasticity points given by σ_0, ε_0 and σ_1, ε_1 in table 4.2 are true strains versus true plastic strains:

$$\begin{aligned} \sigma_{true} &= \sigma_{nom}(1 + \varepsilon_{nom}) \\ \varepsilon_{ln}^{pl} &= \ln(1 + \varepsilon_{nom}) - \frac{\sigma_{true}}{E} \end{aligned}$$

Table 4.2: Material properties [3]

Aluminum 2024 -T3		
E	[MPa]	68563
ρ	[kg/m ³]	2700
ν	–	0.33
σ_0/ε_0	[MPa]	367.5 / 0
σ_1/ε_1	[MPa]	625 / 0.5

4.8.3 Concept A

The concept principle structure consisted of a skin and a mainspar, similar to the cross-section of the SWI between two of the support columns. The outer skin was modeled with an elliptical cross-section with a width of 200 mm and height of 360 mm. The skin was extruded 1000 mm. The mainspar was modeled as a simple flat beam with two flanges down on each side. The mainspar was positioned at 340mm from the nose of the “outer skin”, the same distance as the mainspar on the SWI given in Attachment 3.

The outer skin and mainspar was mid-surface meshed using S4R shell elements and given an initial thickness of $t = 0.8$ mm and $t = 2$ mm, respectively. The element size was set to 10 mm for both the mainspar and outer skin, and both were assigned the material properties of AA2024-T3 given in table 4.2. The skin and mainspar was rigidly constrained to the reference points as shown in figure 4.16. To be able to visually observe the deformation modes, a small strip of the skin face was fastened, instead of just the edge, illustrating an imagined fixture. Two compression tests were performed with two different outer skin thickness; 0.8 mm and 1 mm. This was done to be able to draw some conclusion as to the scalability of force, as was the basis for the concept.

The results from the two compression tests are plotted and shown in figure 4.17 along with the idealized design curve for reference. As we can see, the deformation sequence and the corresponding reaction forces are overwhelmingly in accordance to the assumed deformation sequence. Furthermore, we can see that by increasing the skin thickness of the outer skin, the stiffness and strength are increased in a linear increasing relation. The second rise of reaction forces related to mainspar deformation occurs

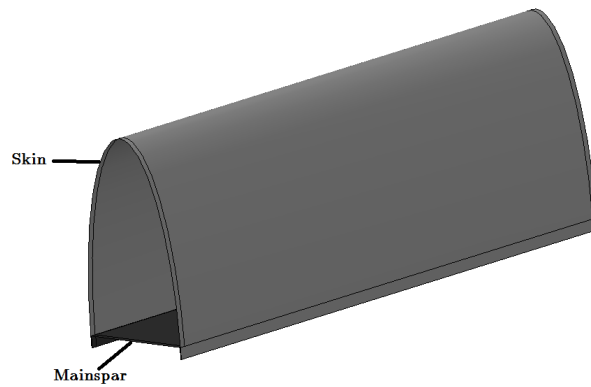


Figure 4.16: Concept A boundary.

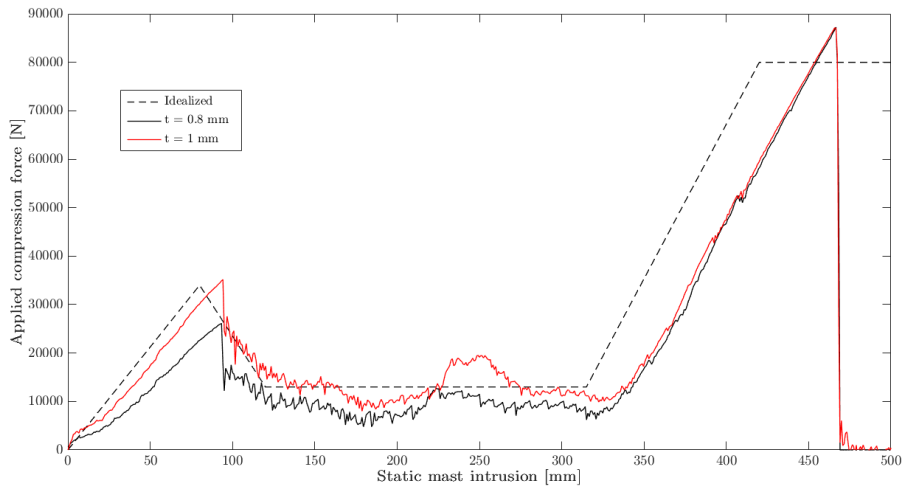


Figure 4.17: Concept A initial compression test.

at a slightly later position than the SWI. This is because the skin was not riveted to the mainspar in this concept for simplicity reasons, and can easily be solved by moving the mainspar to a position, 315 mm from the nose of the outer skin. Furthermore, it is noted that an outer skin thickness of 1 mm seems to be in the same force-range as required for the initial deformation mode, and that a mainspar of 2 mm gives the same relation.

The results may not come as a big surprise, as the simplified model is essentially the same as cutting the deformed piece of the SWI and fixing it on the sides. They do however provide some evidence and confidence in the assumed deformation sequence and forces.

4.8.4 Concept C

Initially concept D consisted of a front beam which produces linear increasing compression forces, an aluminum plate perpendicular to the front beam providing constant shear forces, and a beam representing the mainspar. This particular setup was chosen in order to reduce the number of elements and material consumption in tests, which would both save expensive material and reduce test time

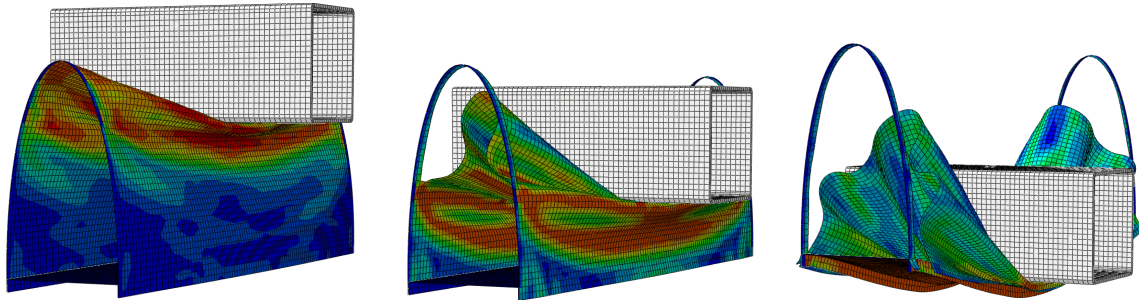


Figure 4.18: Concept A deformation modes.

related to replacement of plates/beams. The initial simulations showed however that the setup was too good to be true. The initial deformation sequence upon impact was as expected and the forces were linearly increasing until failure at a given load. Upon impacting the shear-plate however, the plate buckled sideways due to the large span (1000 mm) between the sidewalls/boundary conditions. This produced a rapidly increasing force way beyond ICAO requirements until failure and stabilized constant shear force. The setup was therefore discarded on this basis. Three different design alterations were considered in order to remove the buckling loads:

1. Introducing notches along the plate's width.
2. Mounting the shear-plates at a tilted angle relative to the front-beam.
3. Pre-buckling the shear-plates by altering the impact geometry or mechanically connecting the front-beam and shear-plates.

Only the pre-buckling alternative showed to have an effect on the buckling load. After several design iterations, I arrived at the setup showed in figure 4.19. The setup consists of a flat aluminum plate as front beam, two plates perpendicular to the front beam and the main-spar. The mainspar has the same design and dimensions as in Concept A and was positioned at 315 mm from the front-beam. In order to pre-buckle the shear-plates, a small strip of aluminum sheet was introduced, connecting the front-beam and shear-plates. In addition, notches have been introduced on each side of the strip to weaken the shear-plate material in the transition between buckling and shear deformation mode. As a requirement it was decided that the front beam should be of 200 mm width in order to physically resemble the SWI. The beam stiffness increases with increasing plate thickness, which also lead to an extremely high ductility. The point of failure and failure loads were therefore not easily controlled. Flaps were therefore introduced at the bearing points in order to predict the point of failure.

The main parameters that were changed through the process were; the width w of the front-beam flanges, thickness of the front-beam and side-plates, depth h_2 of shear-plates, distance h_1 between the front-beam and shear-plates and width of the aluminum strip. Parameters which were kept constant throughout the process were; distance from front-beam to mainspar (315 mm), the distance between the shear-plates and the width of the front-beam (200 mm), mainspar geometry and plate thickness as in concept A.

The front-beam, shear-plates and the aluminum strip was modeled as a single part. The front-beam and shear-plates were then partitioned and given separate section properties, e.g. plate thickness. All the plates were mid-surface meshed using S4R – shell elements with an overall size of 10 mm and given the material properties of Aluminum 2024-T3.

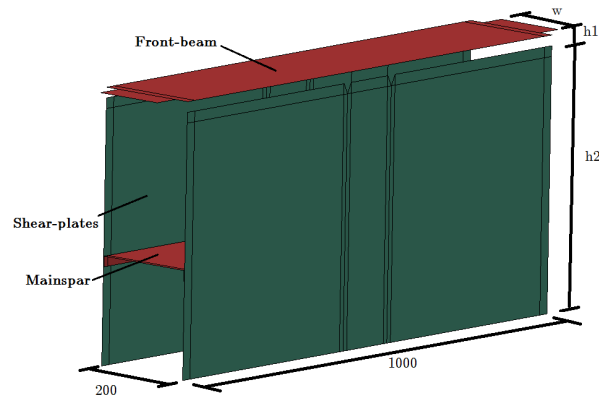


Figure 4.19: Concept C final setup.

Results

The impact response from the design iteration in which the closest relation to the impact response of the SWI/design-curve were achieved are plotted in figure 4.20. The initial deformation mode illustrated in figure 4.21a were buckling of the aluminum strip and shear-plates. This corresponds to the rapid impact force around 10 kN. After the shear-plates had buckled, the front-beam started to deform producing linearly increasing forces until failure at around 39 kN, illustrated in figure 4.21b. We then get a rapid fall in impact forces, and shear-plates starts to shear along it's center as illustrated in figure 4.21c and by the constant reaction forces. After around 260 mm the skin started to stack against the mainspar, as illustrated in figure 4.21d and the forces started to increase as the mainspar start to deform and ultimately failed.

As we can see from figure 4.20 the initial failure point and failure loads are not optimal. The front-beam failed at around 60 mm intrusion, and produced 39 kN reaction forces. This can be adjusted for by reducing the thickness of the plate and the width of the flange on the front-beam. The second rise of reaction force related to skin-stacking against mainspar and mainspar deformation occurred at an earlier impact intrusion (around 260 mm) than the SWI (around 315 mm). The force at mainspar-failure were much higher than the SWI, but happened at the same intrusion depth. Both of these differences are related to the depth of the shear-plates and the distance from the front-beam and the mainspar. The depth $h1+h2$ had to be larger than the distance between mainspar and front-beam, or else the shear-plate were completely sheared before mainspar was hit, which resulted in a sudden drop of reaction forces. This may be accounted for by reducing the thickness of the shear-plates, which would lead to smaller shear forces prior to skin-stacking.

Numerous iterations and variations of plate thickness, distance $h1$, width of aluminum strip, width w of flanges etc. were investigated in order to get the response. The concept turned out to be extremely difficult to dimension which is not easily documented. The idea of separating the deformation modes as done in this concept, turned out to be quite challenging and not straight forward. Some of the most critical design challenge is therefore listed below:

- The failure of the front-beam had to occur at roughly the same impactor deformation as the side-plates starts to shear and at a specified load. This lead to a fairly complex combination of parameters w , $h1$ and plate thickness. In fact, the solution it seemed to converge against were that the shear-plates and front beam was completely joined which would basically lead to the same principle as concept A.
- The front-beam only failed at one side. When the failure occurred, the front-beam still had

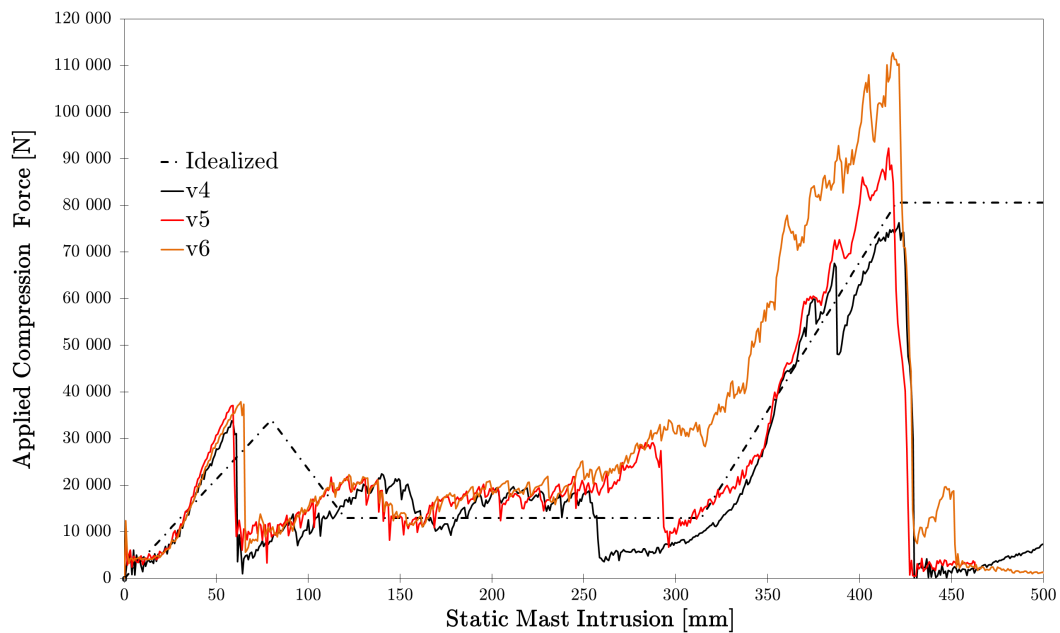


Figure 4.20: Concept C reaction force vs. static mast intrusion.

sufficient structural strength at the opposite side, and started to pull sideways as can be seen in figure 4.21c. This is considered as an undesirable feature in a physical impact test, where the mast impacted would be eccentric impacted. This may however be eliminated at higher impact speeds.

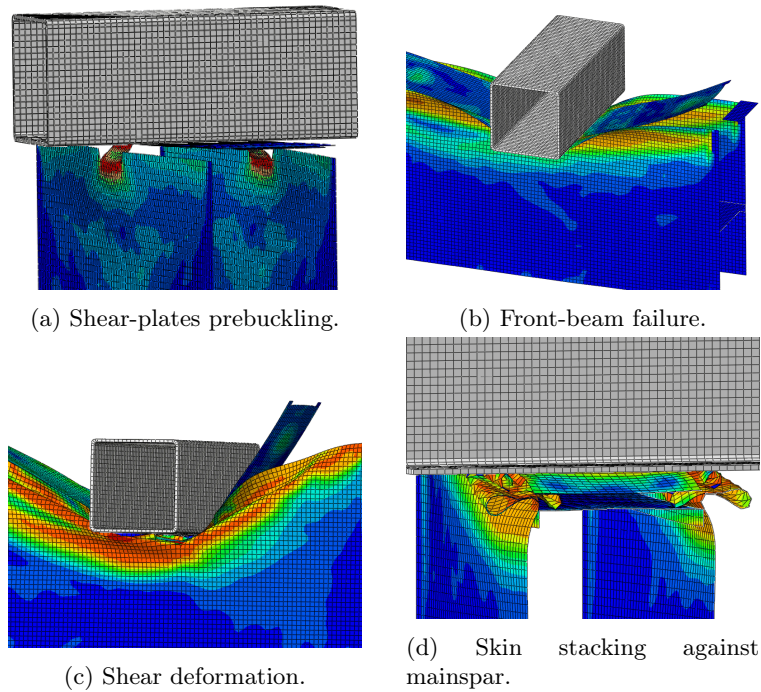


Figure 4.21: Concept C deformation modes.

4.9 Conceptevaluation

In evaluating the individual concept, it is common to do a weighted evaluation of the individual concepts against the specification set in the design requirements. However, as the requirements set in the design requirements for this project are quite vague, it is difficult to weigh the concept against each other. Furthermore, the main goal of this phase was to search for solutions which would give the desired dynamical response, and the conceptual structure are described in more detail than other. The concept evaluation and subsequent choice of concept for further structural detailing will be based on a discussion of each concept.

Concept A showed to comply very well with the desired crush-response, both in deformation modes, force levels and failure at desired deformation. The concept is believed to drastically reduce the material consumption, which in turn reduces cost. A fairly stiff and strong support structure would be necessary to use this, which in turn may increase the cost. One can however make use of more commercially available materials such as steel, which is an advantage with respect to cost. The success of this concept is primarily linked to a good support structure design that provides sufficient mounting and strength as to firmly fix the skin.

Concept B was not simulated, as the skin was the same as in concept A, and the behavior of a spring-mounted plate is fairly predictable at least in a quasi-static analysis. The use of springs instead of the deformable aluminum mainspar as in concept A is considered to add unnecessary costs to the impactor. If the impactor was to be used at a test facility running multiple test a year, this would be a better solution. As the maximum amount of tests that has ever been performed in a single test-program with a soft impactor is 14 [7], and a typical amount around five, the investment related to the spring is considere to be too high as to get any return related to to the reduced material consumption. In addition, the inertia effect of the spring/steelplate is not known and may dominate the results. A fairly complex suspension and/or guidance of the steel plate in order to ensure the axial deformation

of the springs may over-complicate the impactor

Concept D was long time considered as the favorable choice in the conceptual phase. The honeycombs are self-supporting structures, which could drastically reduce the support structure required. The idea of a standardized test-tool which could be ordered from an ICAO-specified supplier/manufacturer was intriguing, as it would give reproducible and comparable results. A lot of time was spent investigating how I could simulate the response of a honeycomb crushing. However, the effect of orthotropic behavior of the honeycombs did reduce the versatility of them, as it requires structural guidance in order to work properly. The loss of strength when crushed bare, i.e. not evenly over the cross-section was considered as a benefit, as it would eliminate the peak forces. A lot of time was used to investigate and look for simple material models and data's which could simulate the dynamic crushing of the honeycombs. Such models were not found, and modelling the entire honeycomb with practically thousands of small cell walls would be computationally impossible. It is however presented as an inspiration for others studying those subject at a later stage.

Concept D had the advantage of using separate plates, which would drastically reduce the complexity of the support structure that is needed. The plates could also be used with small alterations. The simulations showed however that the concept was extremely difficult to dimension as to produce the desired crush force. A solution that was fairly close to the desired crush-response was achieved, but the simulations did not consider the post-necking behavior of the material. The concept also experience some undesired deformation as the front-beam only fail at one end. Furthermore, the concept seemed to converge against concept A. The conclusion is therefore that sufficient confidence in choosing this concept was not achieved.

The chosen concept for further detailing were therefore Concept A: simplification of the SWI. For the remainder of the paper, Concept A will be termed as the surrogate impactor.

Reflection on the method used:

I chose to use a concept generation method that consisted of dividing the individual deformation modes and treat them separately. This worked well in the beginning of the project, to identify different structures that could produce the different crush-responses. The method changed somehow from a structured method, to an iterative process that consisted of proposing a solution, and testing them in simplified models like the ones used in proof-of-concept. It is interesting to see the results from the first steps taken in the five-step concept generation method. Concept D is a direct result of dividing the individual responses and arranging them in such a way that the total crush response mimics the SWI's. Concept C is the direct result from the literature study in the initial steps. The method showed to be somewhat ineffective also, as very few solutions were found to produce the decired response, limiting the number of variations of concepts.

Chapter 5

Embodiment design

Now that we have elaborated the principle solution in the conceptual phase which showed to inhibit the most promising results with regards to mechanical properties, the underlying idea must now be firmed up. In the conceptual phase, some ideas on how to mount the skin to a support structure in order to allow for the replacement of the skin was presented. In this chapter I will structurally detail and dimension the overall layout design. The delivery after this phase will be a complete virtual prototype with dimensions and tolerances which are to be evaluated. In order to detail and design the final solution, the concept was divided into three main areas in which must be detailed:

1. Mounting skin.
2. Mounting mainspar.
3. Support structure

The approach of this phase was to evaluate and determine area's 1 and 2, and then search for a support structure which facilitated the ideal mountings.

5.1 Mounting

5.1.1 Skin

Fixing the skin rigidly to the support structure is considered as one the most challenging task with this design, mainly because of the curved shape, but also due to the underlying idea of the concept of it being replaceable. In the initial concept, the cross-section was semi-elliptical with the same width and height as the distance from the nose-tip to main-spar on the SWI. This shape showed promising mechanical response, but is difficult to easily mount without any complex structural elements. Four different principles of mounting the skin have been investigated:

1. As is.
2. Clamping device.
3. Bent flaps.

The first mounting technique is to use the same principle as the original SWI. In the original SWI, the skin was riveted to a support structure composed of aluminum elements. In this mount, shown in figure 5.1, the skin is bolted onto flanges on the steel support structure. It was considered to keep the aluminum support ribs from the SWI with some small alterations, but was quickly discarded due to

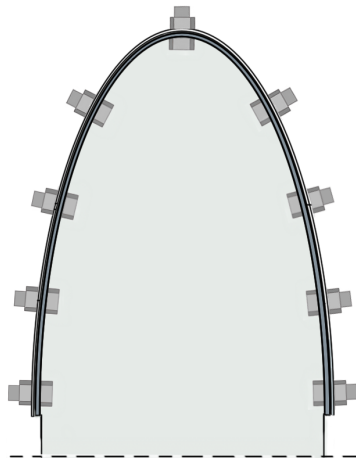


Figure 5.1: Skin mount 1: bolting.

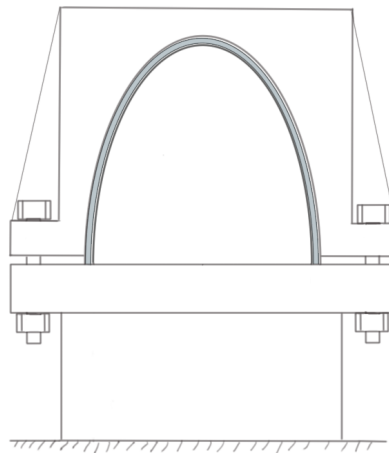


Figure 5.2: Skin mount 2: Clamping device.

material cost and insufficient structural strength. Rivets was also considered as the joining element on the basis that they are easier/faster to fasten, but was discarded due to their low strength. One would also most definitely get rivet failure instead of skin shear when crashed, which are assumed to produce much lower resistance and hence reaction forces. The advantage of using this mount is that it is a very simple setup which requires little custom made parts in order to facilitate the curved shape of the skin. The disadvantage of this setup is that it may require many bolts in order to ensure a smooth failure transition when skin starts to shear. As a consequence the lead time between tests are increased, and replacing the skin may be a tedious task. The second mounting, shown in figure 5.2 is one which facilitates the exact geometry used in the conceptual phase, which are known to exhibit the desired crush characteristics. The setup consists of two components: top module and a support structure. The idea is that the aluminium plate is pre-bent in some order to get roughly the shape desired. The skin is then placed on the support structure which has the width and curvature as the inside of the skin. The top module (the clamping tool) is then placed on top and bolted onto flanges. These two together forms a die onto which the skin is shaped after. The pressure that it produces creates frictional forces, holding the skin in place. There are though several disadvantages of utilizing this clamping device:

- The Force at which must be applied are greatly affected by the plate thickness and size, and are assumed to be high.
- Tolerances must be quite strict to ensure adequate mounting.
- Complex structural elements.

These can all be accounted for, but at the possible effect of higher production costs. An advantage with this design is that little alterations, such as drilling holes, has to be done on the skin and process of changing the skin after a test is much quicker and easier than for the bolted skin for instance.

In the third setup, the geometry of the impactor is altered slightly from the initial proposed in the concept phase in order to facilitate easier mounting. Instead of a smooth curved elliptical shape, the side-walls and nose are straight and . This allows us to fix the skin to the support structure, using simple plates and bolts. Figure 5.3a shows the altered geometry and the third method to fix the skin to the support structure. The skin has pre-cut flanges, which allows us to bend the skin over the support structure as indicated by the arrows. By doing so, the reaction forces that the mount must withstand are drastically reduced. The only force it must withstand is the up-wards pulling forces which are generated by the bending moment generated by the force F_y , which is considerably smaller

than for mount 1 and 2.

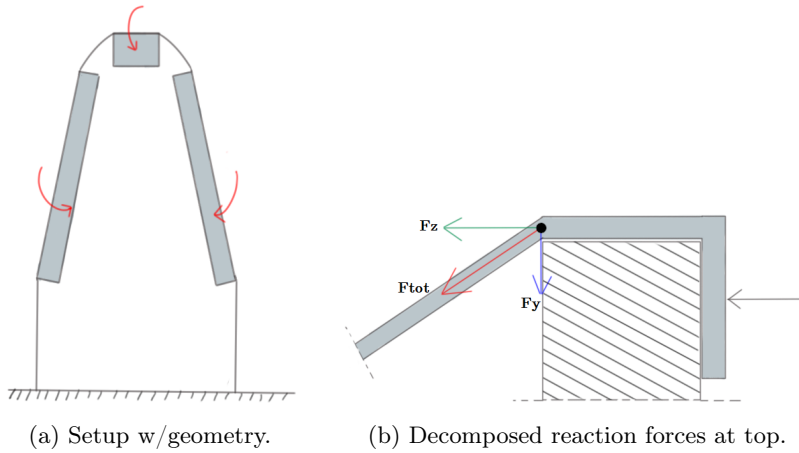


Figure 5.3: Mount setup 3.

5.1.2 Mainspar

The mainspar is designed as in principle a simple beam, and the mounting of the mainspar is considered as a relatively simple task in relation to the complex shape of the outer skin. However, the forces which the mount must withstand are of a much larger character. Since the concept is based on the fact that only the mainspar beam and skin are to be replaced between tests, the challenge is therefore to design a mount which is both strong and facilitates easy assembly and dis-assembly. Several different setups have been investigated, and three of the most promising are presented:

1. Slot mount.
2. Flange mount.
3. Combination of 1. and 2.

The first mainspar mount, shown in figure 5.4, consists of a plain aluminum plate which is fixed at each end through slots in the support structure. The idea is that when mounted, the plate is slid through both slots and bent downwards on each side. This creates the same reduction of clamping forces required, as described in skin-mount setup 2. Some sort of fixture to hold the plate flat on the outside has to be provided. This is considered as a simple and effective mount with respect to both structural strength and assembly, but the introduction of slots in the support structure adds complexity with regards to production.



Figure 5.4: Slot mount mainspar.

The second mainspar mount, shown in figure 5.5, consists of a plain aluminum plate which is placed between two flanges on each side of the support structure. The aluminum plate is held in place with a

steel plate and two bolts. The mount is simple in construction and thus production, and the assembly and dis-assembly is considered as to be easy. The pressure that must be applied by the steel plate, and subsequently the bolt loads, to ensure sufficient frictional to fix the mainspar are much higher than for mount 1.



Figure 5.5: Flange mount mainspar.

The third mainspar mount consist of a simple aluminum plate which is pre-bent at the workshop before testing. The mount is shown in figure 5.6 with two different bolt configurations. The pre-bending creates a flap at each end onto which the plate is fixed to the support structure with a steel plate and two bolts. When mounting the mainspar, the flaps are placed in the slot created between the bolts and the plate. The four bolts are then tightened using a wrench to a designed moment. The plate acts both as bedding for the cross-beam, and as clamping device for the flaps. The mount is considered as strong and easy to assembly/dis-assembly, but the pre-bending of the aluminum plate introduces an additional production process which increases the cost. That being said, the mount also simplifies the support-structure design in contrast to both slot and flange mounts.



Figure 5.6: Main spar mount 3 configuration.

5.1.3 Chosen mount principles

Initially, a combination of skin mount 1 and 2 in combination with mainspar mount 3 was chosen as shown in figure. By making the front of the skin flat, and introducing flanges on the each side, the skin was to be bolted firmly on the flanges as illustrated in figure 5.7. This particular setup was initially considered as a superior choice based on the shear simplicity of production and assembly. Also, the setup superiority was further enhanced by some initial bolt calculations which showed that the bolt loads were feasible with respect to strength. These bolt load calculations showed however to greatly underestimate the required pressure on the plates, after a quasi-static crush simulation was done in ABAQUS. New bolt loads were calculated to be in the range of 100 kN per bolt as shown in attachment 3, which meant that the bolt either had be of a large size (M20) or of a high strength. In addition, the torque required to fasten the bolts would be The setup was therefore discarded on this basis, and a re-evaluation of the entire setup was necessary.

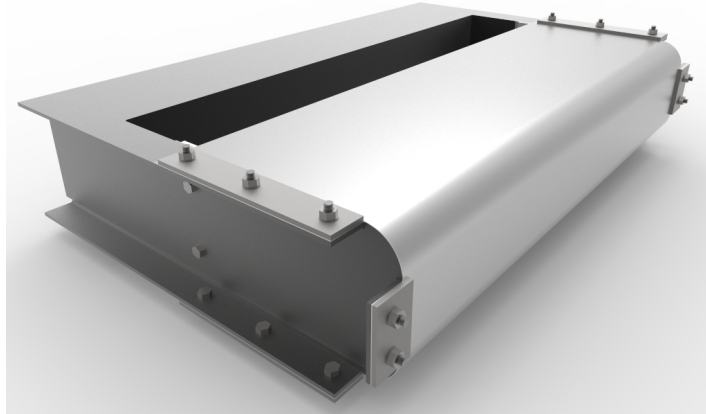


Figure 5.7: Finalsetup version 1.

Based on the large inwards pulling forces in which the mount must withstand, and with the experiences obtained in the development and analysis of the failed initial setup, the skin mount 3 and mainspar mount 1 were considered to be the only setup which were able to provide sufficient structural strength with fairly simple elements.

5.2 Optimilization – Geometry

In the conceptual phase the cross-section of the outer skin was modeled with an elliptical cross-section. This was done because it was in close relation with the shape of the SWI. This geometrical shape showed at an early stage to be particularly difficult to mount without using complex and heavy-duty fixtures as discussed earlier.

The chosen mount required that the front and side-walls on the support structure (and skin) had to be straight. In addition, the straight sidewalls are easier to build and bend during construction. To optimize the cross-section of the skin, the same setup and simulation approach which was used in section (referrer) was utilized to determine the dimensions. The results from the simulations in the conceptual stage showed that a skin thickness of 1 mm produced the desired shear-forces of around 13 kN. The skin thickness was therefore kept constant at 1 mm.

The skin are to be fixed along the side-walls and at the top, as indicated by the red lines in figure 5.8. The distance between the side-walls at its widest was decided to be the same width as the largest width of the SWI of 200 mm. The depth of the skin was kept constant at 340 mm, which is the distance between the mainspar and the front tip on the SWI. It should be noted that this depth does not have any influence on the first deformation modes, and could be increased/decreased.

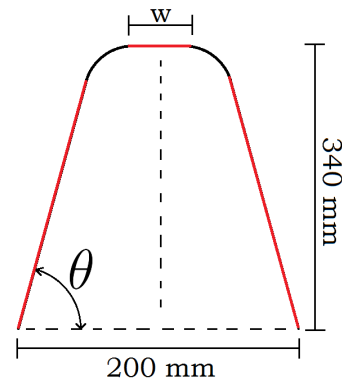


Figure 5.8: Cross-section optimilization.

By constraining the arch connecting the top flange and sidewalls to be tangential, the only parameter that was altered in this geometry optimization were the width (w) of the top flange mount. The

angle was θ was automatically determined by the tangential constraint. In the initial iterations it was assumed that the overall shape had to be as close to the elliptical one in the conceptual phase as possible. By running several iterations I ended up with a flange width w of 100 mm, which resulted in a peak load of 32 kN at 90 mm intrusion. This led to a θ of 90 degrees meaning that the side-plates are positioned perpendicular of the flat front-end. This is considered as a great advantage in the production of the support structure.

5.3 Support structure

The development of a support structure based on the mount principles chosen showed to be a somewhat challenging task. The considerations, requirements and challenges that was encountered and set are summed up below:

- The space between the support structures side-ribs, which is the space in which a mast would penetrate, cannot have any structural element except the deformable mainspar.
- The support structure had to withstand the large bending moment generated during the initial deformation mode. As a minimum, no yielding should occur during impact.
- The inwards deformation at mainspar mount should be minimal.
- The absolute minimum theoretical distance from top of the support structure to the bottom were 420 mm. Additional space should be added in order to allow for complete failure of mainspar.
- Mainspar must be mounted in the center of the support structure.
- Support structure must provide bedding and mounting for the skin and mainspar.

Several different designs were considered in this process in order to land on the optimal solution. Simple static analysis was performed in order to evaluate the strength and stiffness of the different variants. Two types of structures became however pre-dominant, each based on different structural elements, and several variants of the layup was considered. Figure 5.9 shows a support structure which is composed of a set of rectangular steel tubes arranged and welded in order to provide the sufficient strength and layout. Effort was made to limit the number of tube dimension and use standardized tube dimensions in order to reduce cost by ordering stock products. More specifically: the ribs, skin-bedding and mainspar-bedding are all tubes of same size whilst the main support tube is separate. The setup is considered to be easy to produce, as the only manufacturing methods that is needed consist of cutting the tubes in the desired lengths and welding/bolting them together.

Figure 5.10 shows a design similar to the SWI. The ribs is a 20 mm thick steel plate and acts as both bedding and mounting for the skin and mainspar. A gap has been introduced in the center of it to allow for mainspar mounting. The ribs are supported by two relatively thick 10 mm steel plates side-support plates to withstand the large bending forces. In addition, a small triangular steel-plate has been added to distribute the forces at the bottom and added stiffness. The ribs and side-supports rests on a square steel tube with the outer dimensions of 200 x 200 mm. The design relatively simple in construction, but does require the use of thick steel plates which adds substantial weight and possibly increased cost. This was however necessary in order to provide sufficient strength and stiffness with combination of structural simplicity. It should be noted that effort was made to optimize the steelplate-structure using thinner plates by adding structural elements to stiffen and distribute the forces. The structure then became overly complex, and was discarded on the basis that it would presumably increase the cost. Furthermore, the ribs could also consist of two 10 mm plates which are joined together, and only one plate-dimension are necessary. This design is also the one which are closest to the conceptual mounts.

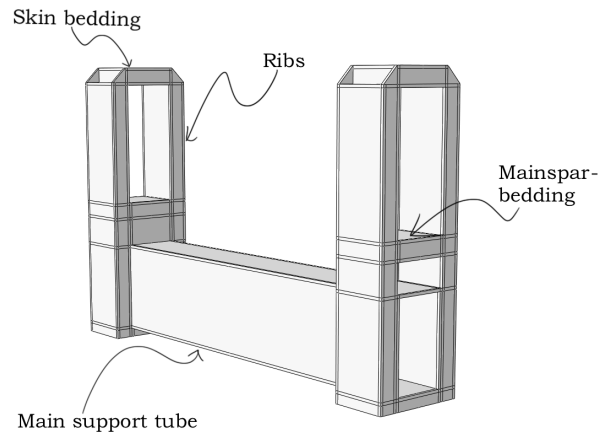


Figure 5.9: Tubular support structure.

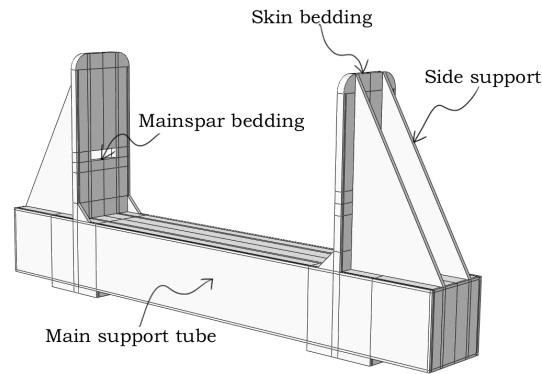


Figure 5.10: Steel plate support structure.

5.3.1 Statical analysis

Learning from the mistakes with the first version, a statical analysis was conducted in order to validate if the two support structures are able to withstand the large forces. The analysis was performed in Abaqus 6.12 Standard. To simulate the forces, a pressure force was applied to the top of the ribs, with a total of 10 kN. A concentrated force of 60 kN was applied to a reference point at the inner end of the ribs. The reference point was locked with the top surface of the ribs with MPC's. These force-levels were taken from the geometry optimization simulations, where the boundary conditions were altered in order to read the forces at bearing points. These were max 53 kN on the top in the transverse direction, and 7 kN in the axial direction. As we can see from figure 5.11 the maximum stresses were 370 MPa and 380 Mpa for the tubular and the steelplate structures, respectively. The maximum deflection at top for the tubular structure was 2.69 mm and 2.17 mm for the steelplated structure. The steel-plates was therefore stiffer, but had higher tensile stresses at critical points than the tubular where the highest stresses were compression. A steel with a yield strenght of minimum 420 MPa has to be used for this setup. This is a fairly high-strength structural steel which may not be as readily available as the more common 369 MPa.

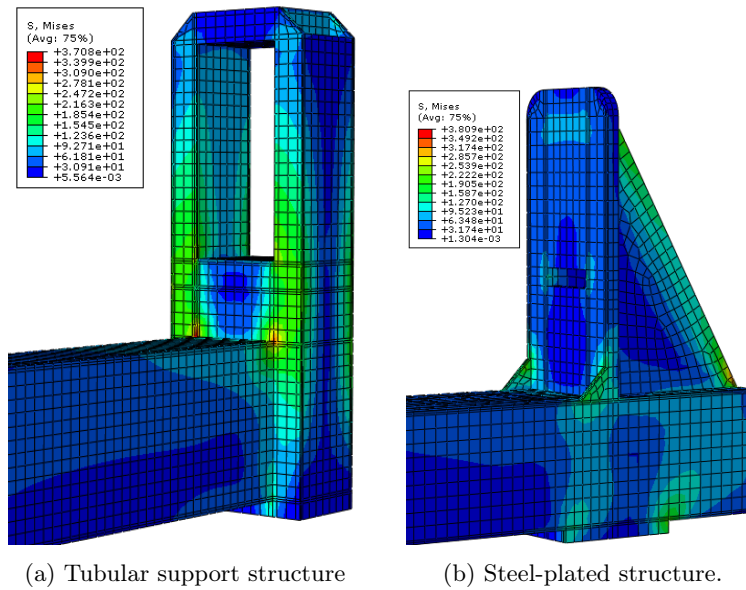


Figure 5.11: Static analysis results.

5.3.2 Discussion/chosen support structure

These results presumably favors the tubular support structure. However, the surface area which the square tubes of 120x50 mm inhibits, could lead to the skin regaining some strength after initial failure of mount flanges. This was observed in an initial compression test with this design, leading to skin tearing after. The decision was then made to use the steel-plated support structure as a preliminary prototype for the verification of the product. A optimization of the structure should however be done in order to bring the thickness of the plate down, as 20 mm ribs is a massive lump of steel which would be heavy and difficult to mount on a truck. Such a structure was not identified in this work although.

5.4 Final version

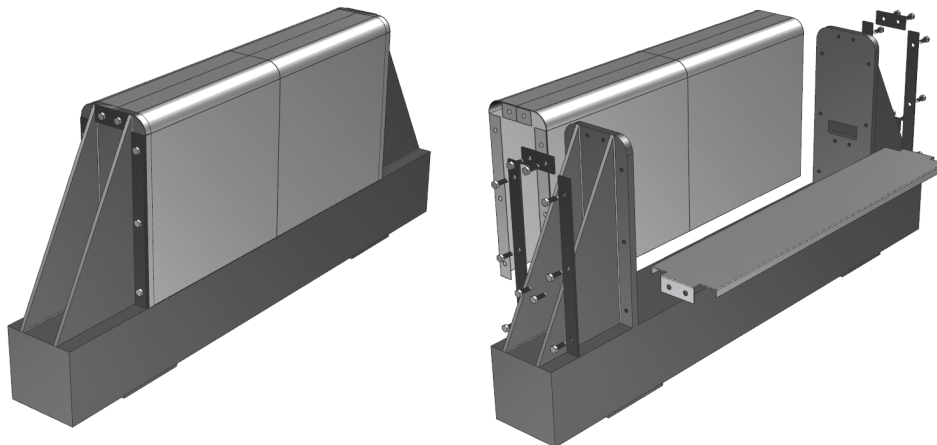


Figure 5.12: Proposed solution assembled and exploded view.

The proposed solution are shown as assembled and exploded view in figure 5.12. It is composed of the support structure, skin, mainspar, sideclamps and top and mainspar clamps. The dimensions of the individual components are given in attachment 5. In order to fix the mainspar to the support structure, flaps has been introduced here as well. The mainspar is the same width and dimensions as the one in the SWI. It was decided to use the same width to provide support at the side-walls of the outer skin upon impact. A simplified version which had the width over the entire length was considered. It was however discovered in the conceptual phase that it had an great effect on chrush response, whether the mainspar had sidewalls which the skin could “rest” against. During compression the skin will buckle and stack several times as the intruder chrushes. Without anything constraining the skin in at least one direction, the skin would experience large sideways deformation. The introduction of flanges was necessary in order to mount it to the support structure. The skin thickness of the mainspar was increased to 2.5 mm in order to account for loss of strength regarding this alteration. The skin is fixed by three steel plates, which are bolted onto the support structure. Ideally nuts and washers would be used, in order to account for any deformation the structure may experience during impact. It is however impossible to mount the skin with nuts on the inside, as the skin blocks the passage. It was therefore decided to thread the holes on the support structure. Another possible solution is to increase the height of the hole which the mainspar is mounted through which the inside of the structure is reached. The proposed setup consist of in total: twenty bolts, four skin-mounts type large, four skin/mainspar-mount type small, one skin, one mainspar and the support structure. The bolts can be bought stock for a fairly small price, and are readily available while the rest of the components are essentially custom-made. The reduction of cost with this setup is limited for small amount of tests, but linearly increasing with test numbers. It is however assumed to be much more predictable and insecurities such as production method of the SWI is neglected.

5.4.1 Assembly/production of consumables

In the presentation and discussion of the mounting of the mainspar and outer skin, the fundamental idea was to pre-cut the flanges on the skin and bend them onsite. If this is the case, the skin must be bent over the outer ribs at each end, and over the entire support structure. It may have been greatly underestimated the forces required to bend the 1 mm aluminum skin without any special tools. Especially for the flaps which the skin is bolted onto the support structure ribs, as the moment generated by the 30-40 mm flap are far less than when the 400 mm sides are bent down on each side of the support structure. This may be resolved by pre-bending the flaps as shown in figure 5.13. Figure 5.13 also shows how the skin is pre-cut in order to create flanges which are bolted onto the support structure. The initial idea was to bend the skin over the support structure on-site as shown in figure

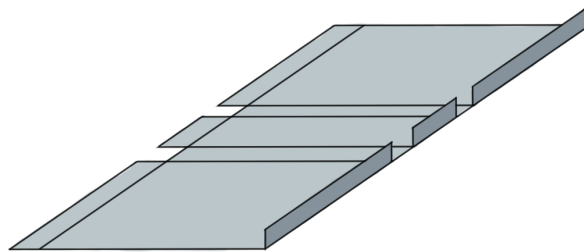


Figure 5.13: Pre-cut and bent sheet.

5.14a. The skin could be bolted onto the top flange and then bent down on each side. As mentioned, it is somewhat uncertain whether this is possible to do because of the stiff aluminum plate. The support structure creates a bedding for the overall shape of the skin, and by pre-bending the flanges on the skin it is considered to be adequate lateral stiffness as to not get undesired deformations of the skin.

However, when forming sheet metal the sheet has to be bent at a slightly greater angle than desired, as it will retract upon unloading due to the elastic bending. The method described might induce additional strength as the skin is in fact pre-stressed. An alternative method of bending the skin is shown in figure 5.14b. This method is done prior to the testing is done, typically during construction of the support structure. It consist of bending the skin over a metal or wooden cylinder with an radius of 50 mm

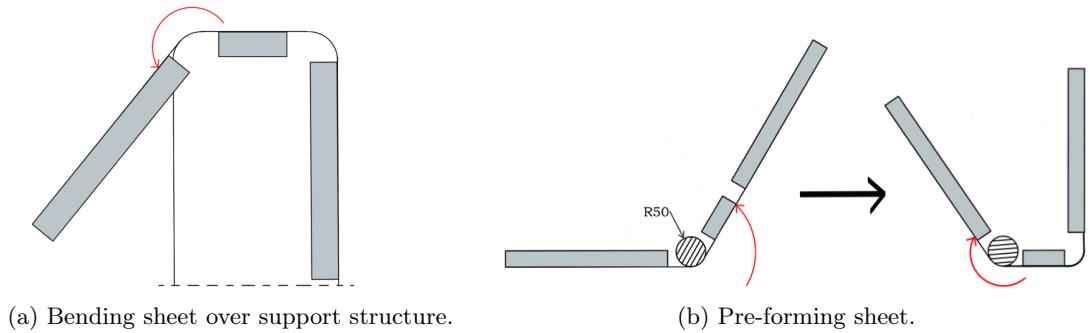


Figure 5.14: Aluminum skin forming methods.

The chosen production method is entirely up to the user preferences, but the method of bending the skin over the support structure is considered to be easier as the tool is already there. The other method could however simplify the support structure additionally as the fillet on the top corners of the ribs would not be necessary.

Chapter 6

Product simulation

The proposed impactor are to be used in future physical high-velocity crash test to evaluate the frangibility of airport masts. The surrogate impactor properties should therefore be verified and benchmarked in order to verify whether it is an adequate substitute to the SWI, and to what degree. The ideal approach would be to perform a physical full-scale high-speed test with a frangible mast similar to earlier test programs such as [21]. This is however very expensive, and the profitability of doing such is considered to be minimal. Quasi-static compression tests are however much more cost-effective and can be done in controlled environment. A quasi-static compression test setup was therefore chosen to identify and benchmark the mechanical properties to the tests performed by [3] and [2]. A dynamical compression test was chosen in order to investigate effects causing inertia and damping forces are taken into account, which was not investigated on a conceptual stage.

All simulations were performed in Abaqus/Explicit version 6.12-1. The quasi-static compression test should presumably favour the Implicit solver as the Explicit solver requires large number of increments. The complex contact algorithm could however not provide a stable solution. The Explicit solver was therefore used in both the static and dynamic simulations. In total of four quasi-static test was performed in order to investigate the effect of material modeling and material strength. In addition a quasi-static compression test with an eccentric loading was performed to investigate the surrogate sensitivity to impacts off it's center line.

6.1 Material modeling

In the conceptual phase, a bi-linear material model was used to describe the strain hardening portion (b-c) of the stress strain curve. It was used as a rough estimate, as it was considered as not important to get an accurate crush-response when evaluating the individual concepts. It is however believed that the strain hardening behavior of the material have an significant impact on inelastic buckling and crushing behavior of metal structures [3]. It was therefor decided to use a non-linear material model as well as the bi-linear in the study of the final product. The non-linear material model used is the continuous model established by Ramberg-Osgood. It provides a single smooth curve for all values of σ and does not exhibit a distinct yield point. The ramberg-Osgood relationship is given by:

$$\varepsilon = \varepsilon_e + \varepsilon_p = \frac{\sigma}{E} + \left(\frac{\sigma}{H}\right)^{\frac{1}{n}} \quad (6.1)$$

in which ε_e and ε_p are the elastic and plastic strain, respectively, n is the strain hardening exponent and H is a material constant which are determined by the offset yield strength [25]:

$$\sigma_{0.2} = H(0.002)^n \quad (6.2)$$

Table 6.1: Material properties

Property	Aluminium 2024-T3 [3]	Structural Steel [26]
Young's Modulus [MPa]	68563	207000
Poisson's ratio	0.33	0.27
Yield strength [MPa]	367.5	572
Ultimate strength [MPa]	435 @ 10 % strain	717
Fracture strain [%]	15	27
Density [kg/m^3]	2700	7680

The same method of fitting the two models through two defined points on the experimental data for the aluminum 2024-t3, as described by [3] was applied. It should be noted that this was not performed by the author of this report, as the data's were kindly provided by prof. Terje Rølvåg for this analysis. The post-necking portion of the stress strain curve (c-d) has not been considered or any other parameters. This strategy of defining a maximum allowable major strain and relate this to a separation cutoff level at single node level in the numerical algorithm may be an oversimplification. This was although necessary as access to sophisticated material data and knowledge about damage modeling techniques was limited. The results should therefore be interpreted accordingly, but may serve as an indication. Numerical simulations are rarely any accurate means to predict highly non-linear deformations such as the crush response of a structure, and often over or under- estimates the true physical response. Typically, the numerical models are used to a posteriori capture the crash-response, and parameters are tweaked in order to fit the physical world. It was therefore considered to be a futile effort to study the effect of parameters such as ductility, as no further conclusions could be drawn without anything to benchmark against. Furthermore, the failure of the surrogate impactor is fairly predictable as it has introduced failure points (flanges), and it is a fairly good assumption that by increasing the fracture strain, the strength is increased.

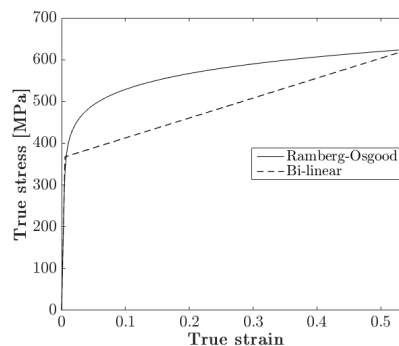


Figure 6.1: Material hardening models.

The skin thickness was instead chosen as the other parameter to investigate. The skin thickness is along with the strain hardening believed to have a great influence on the buckling of side-walls, and thus the produced reaction forces, especially for the dynamical impact test.

6.2 The model

6.2.1 Parts/mesh/material

The surrogate impactor was modeled in ABAQUS part module with the dimensions given in Attachment 4. This was done despite a model was originally modeled in NX10.0 to allow for easy alterations of dimensions and addition of structural elements if it be required. There are some uncertainties related to the strength of the skin and mainspar due to the altered boundary conditions and dimensions which was necessary for the assembly of the skin and mainspar. The parts were modeled individually and assembled in the assembly module in ABAQUS. Taking advantage of symmetry, only a quarter of the individual parts were modeled and mirrored twice.

The skin and mainspar was modeled as a 3-dimensional deformable shell with the dimensions given in Attachment 5. The mainspar and skin was meshed with S4R – top surfaced elements with an element size of 10 mm and a thickness of $t = 2$ mm and $t = 1$ mm, respectively. Both were assigned with the material properties of Aluminium 2024-T3 given in table 6.1. The top-surfaced mesh was used for convenience reasons (simplified modeling). The support structure was modeled as a single 3D solid,

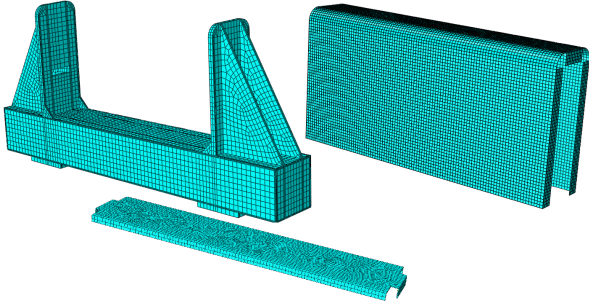


Figure 6.2: Meshed parts.

which eliminates any material weaknesses related to the welding of the individual components. This element was not considered in this study as the main purpose was to document the crush-response of the surrogate impactor. It was meshed with C3D8R elements with an overall element size of 20 mm. Mesh-refinement was done on the fillet between the rib top and side to avoid conflicting surfaces with the skin. The support tube was assigned with the material properties of steel as given in table X. The skin and mainspar was modeled as a shell and meshed with T4R shell elements with a thickness of $t = 1$ mm and $t=2$ mm respectively. The individual parts with mesh are shown in figure 6.2.

6.2.2 Assembly FEM/boundary conditions

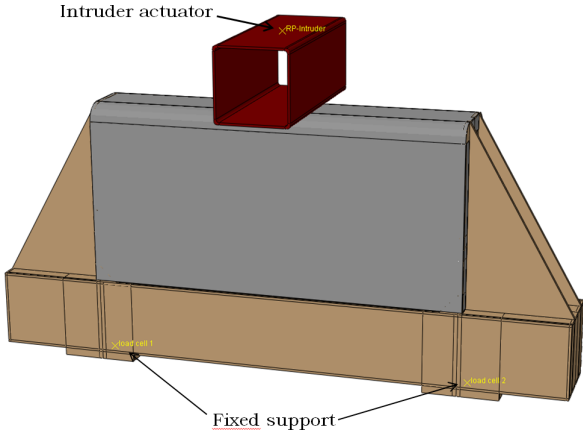


Figure 6.3: Assembly/test setup.

The assembled components and test setup is shown in figure 6.3. The intruder was centered between the outer support ribs on the quasi-static compression tests and dynamic impact tests. In the eccentricity test, the intruder was position with its centerline 200 mm from the centerline of the surrogate impactor giving an effective distance of 200 mm from the outer rib.

The support structure was fixed at the two load cell points through two reference points. This allows us to record the reaction forces and moments generated in the dynamical impact test, in compliance with the ADM recommendations. The reference points and the bottom of the support structure were connected through MPC type BEAM as shown in figure ???. This corresponds to the presence rigid beams, constraining the displacement and rotation of the nodes on the bottom surface to the reference point's displacement and rotation [6]. The reference point was constrained in all rotational and translational directions.

The intruder was defined as a rigid body, whose motion are governed by the motion of the rigid body reference node named RP-intruder in figure 6.3. A constant velocity of $v = 55 \text{ mm/min}$ and $v = 140 \text{ km/h}$ was applied on the reference point in the quasi-static and dynamical compression test, respectively. By setting the velocity equal to zero in all rotational degrees UR1, UR2,UR3 and transverse directions to the impact direction, the rigid body was sufficiently constrained, allowing only movement in the axial direction.

In order to reduce the simulation time and complexity of the model, the bolts and plates which constrain the skin and mainspar to the support structure were not modeled. The stable time increment is related to the smallest element size in the assembly, and bolts would require a fine mesh. The skin and mainspar was instead fixed to the support structure by using a surface-based shell-to-solid coupling. This also allows using a coarser mesh on the support structure as it does not require any alignment between the solid and shell element meshes [6]. The skin was partitioned so that the constrained nodes were positioned 2 mm from the bent edges, which would account for any shear failure. The constrained nodes are shown in figure 6.4. Before this method was used, and to be confident that it does not mask any problems such as slipping between pretensions plates and skin, a analysis of the bolt connection at the top was performed which is given in Attachment 5. The results showed that the solution was feasible with sufficient bolt loads, which were well within reasonable limitations.

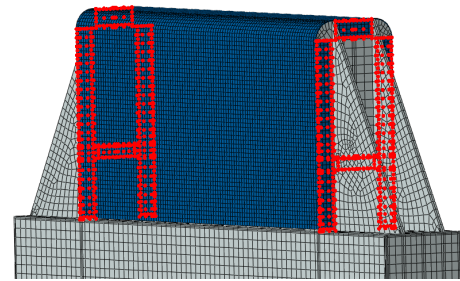


Figure 6.4: Constrained nodes.

6.2.3 Reducing computational costs

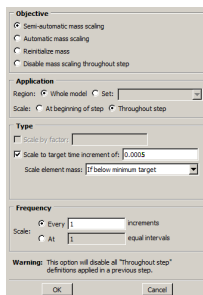


Figure 6.5: Mass scaling definition.

As mentioned earlier, the Explicit solver requires a large amount of increments to perform an analysis. The computational time involved in running a quasi-static analysis can therefore be very large, since the cost of simulation is directly proportional to the number of time increments required [6]. The computational cost may be reduced by either speeding up the loading rate (higher intruder velocity) or scaling the mass. As the compression test [2] and [3] was performed with an intruder velocity of 50 mm/min , it was decided to use this in the analysis.

Mass scaling reduces the number of increments, n , by artificially increasing the material density ρ [6]. It has the same effect on the inertia forces as increasing impactor velocity, but can be used in rate-dependent problems.

Mass scaling should however be used with care to ensure that the inertia forces do not dominate and change the solution. The mass-scaling was therefore set to a minimum level as to get as realistic data's as possible at an acceptable computational efficiency. The results should be interpreted

6.3 Results

In total of four quasi-static test and four dynamical tests was performed, each material model with a skin thickness of $t = 0.8$ mm and $t = 1$ mm.

6.3.1 Static compression test

Figure 6.6 shows the results from a skin thickness of 1.0 mm. The deformation modes of the non-linear material model and bi-linear material model is documented in figure 6.9. As we can see from figure 6.6, the first deformation mode yielded the desired stiffness. Both material models failed at approximately the same mast intrusion, but the non-linear material model gave much higher strength in deformation mode 1 with a peak load of 35 kN vs. the 27 kN for the bi-linear. The top flanges on the skin failed at both ends simultaneously for the bi-linear model, while the non-linear material model caused failure at only flange. This was due to localized buckling as shown in figure 6.9, preventing the deformation of skin on one side. The skin then started to shear on the side that had failed, while the other flange still had it's structural integrity. This In turn led to sideways sliding of skin under the intruder as it continued to compress downwards. The drop of forces at around 180 mm mast intrusion for the non-linear material model is related to complete skin failure at the other side as well. The bi-linear material model on the other hand yields the desired constant crushing force and force levels for deformation mode 2, but regains some strength at around 200-250 mm mast intrusion. This is also observed for the non-linear material model and are related to the skin bending inwards and resting against the mainspar. The last deformation mode related to skin stacking against mainspar and mainspar deformation and ultimately failure occurred at the desired mast intrusion and the stiffness is equal for both material models. The non-linear material model gave however again much higher strength at failure, with a peak load of 56 kN as opposed to the bi-linear which failed at 44 kN.

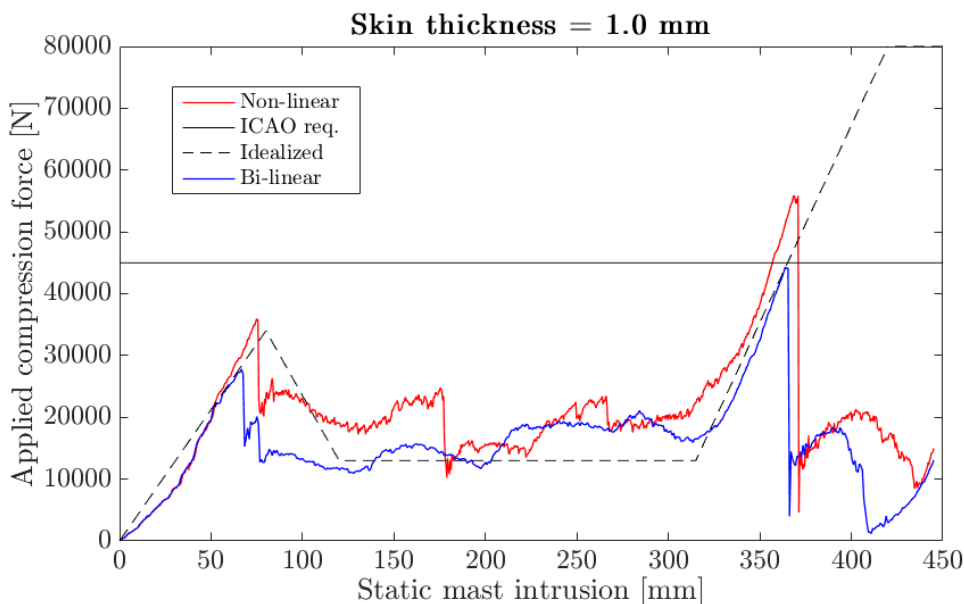


Figure 6.6: Force versus static mast intrusion, skin thickness $t = 1$ mm

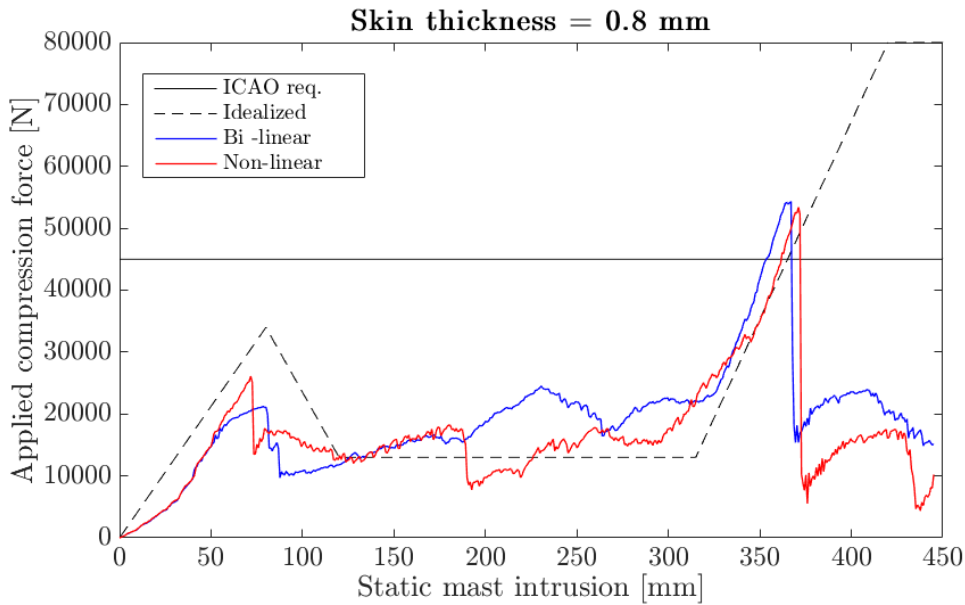


Figure 6.7: Force vs. static mast intrusion, $t = 0.8$ mm

The same deformation modes (figure 6.9) were observed for both material models with a skin thickness of 0.8 mm as for 1 mm. For the non-linear material model, the reduction of skin thickness led to a seemingly linear reduction of force levels recorded as shown in figure 6.7. However, the secondary failure of the remaining top flange did occur at a slightly deeper mast intrusion, which indicates that the 0.8 mm skin thickness is more ductile. For the bi-linear material model, the differences in recorded compression forces are more imminent. After initial linear-elastic deformation and subsequent failure, the 0.8 mm skin thickness exerts a linearly increasing compression force in the 100-230 mm mast intrusion range. This is probably due to lowered resistance for buckling, causing the skin to stack in an orderly and denser fashion, as shown in figure 6.8. The peak force related to main spar failure was as expected lowered for the non-linear material model, but was in fact increased for the bi-linear, resulting in an equally large peak load of around 54 kN. The increased peak load for the bi-linear material model is due to the more ductile behavior with a skin thickness of 0.8 as opposed to 1 mm, which led to increased skin stacking against the main support tube, as shown in figure 6.8.

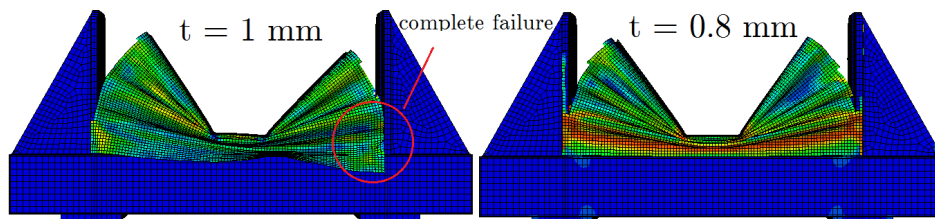


Figure 6.8: Degree of skin stacking against main support tube.

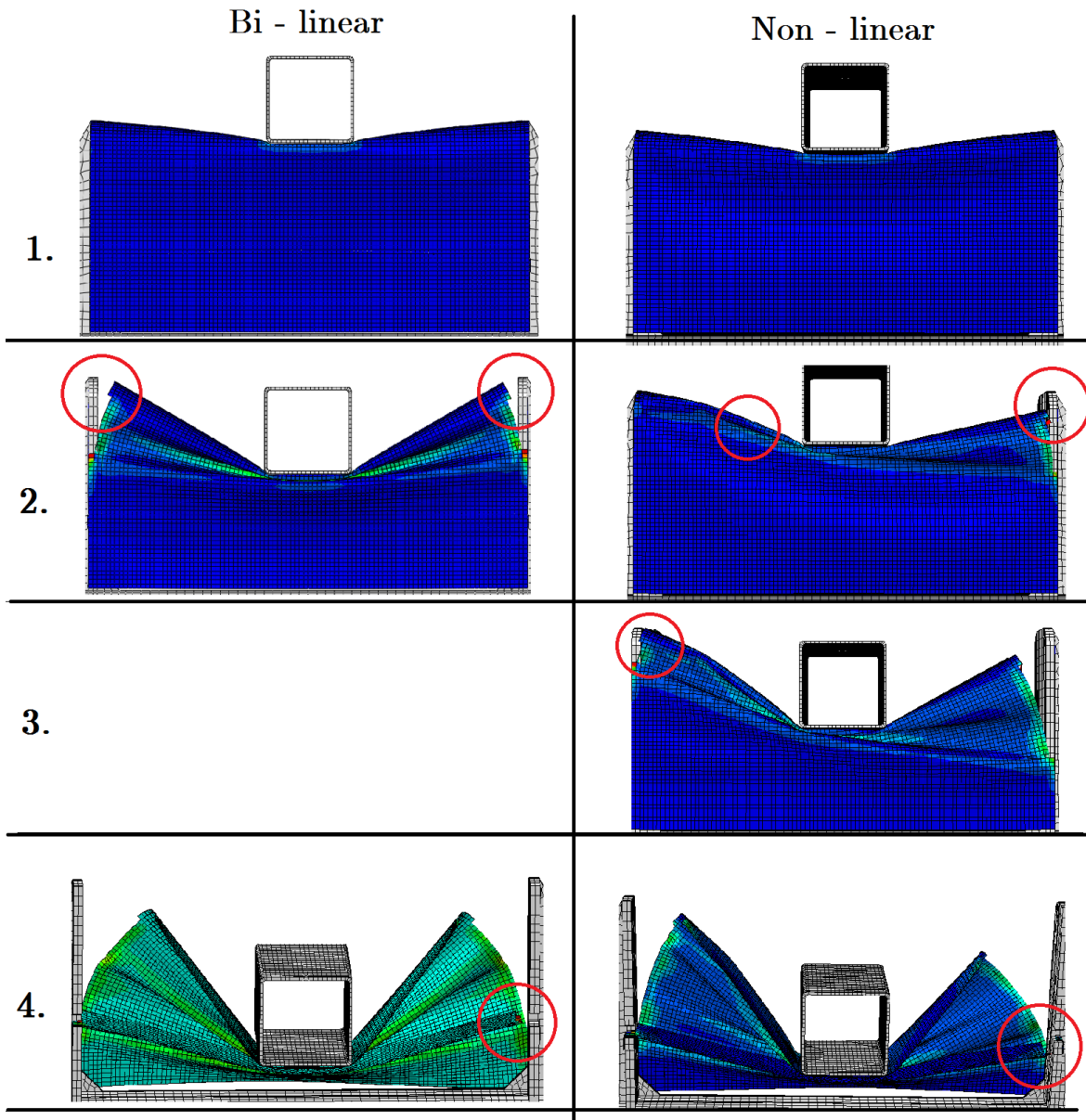


Figure 6.9: Quasi - static deformation modes.

Comparing the results from the quasi-static analysis with the compression test in [3], figure 6.10 shows that the non-linear material model with a skin thickness of $t = 1$ mm gives initial reaction forces in the same force-range as for the SWI. The following deformation mode was slightly altered, and thus not recorded forces are indifferent. When the flange finally did fail the force-levels and stiffness were in very good relation with the SWI. The bi-linear material model gives a more comparable failure modes, but the peak load at initial failure were a little low. The following shear deformation mode and force-levels conforms very well with the equivalent deformation modes and recorded crushing forces for the SWI. The mentioned slight increase of forces at around 250 mm were in fact also observed for the SWI. The stiffness of the mainspar are in good relation with the stiffness of the main front spar of the SWI, but the strength is around half the strength of the SWI for the bi-linear and slightly less for the non-linear.

This is greatly dependent on the fracture strain of the material, and since the post-necking behaviour of the material has not been considered in this study, the strength is expected to increase some. The reduction of the flange width on the mainspar is however the main factor for this reduction of strenght, and may be reconsidered. However, the non-linear material model gives reaction forces exceeding the ICAO requirement, and the bi-linear are very close to the 45 kN frangibility criteria. The setup may thus be used to determine the frangibility of a mast.

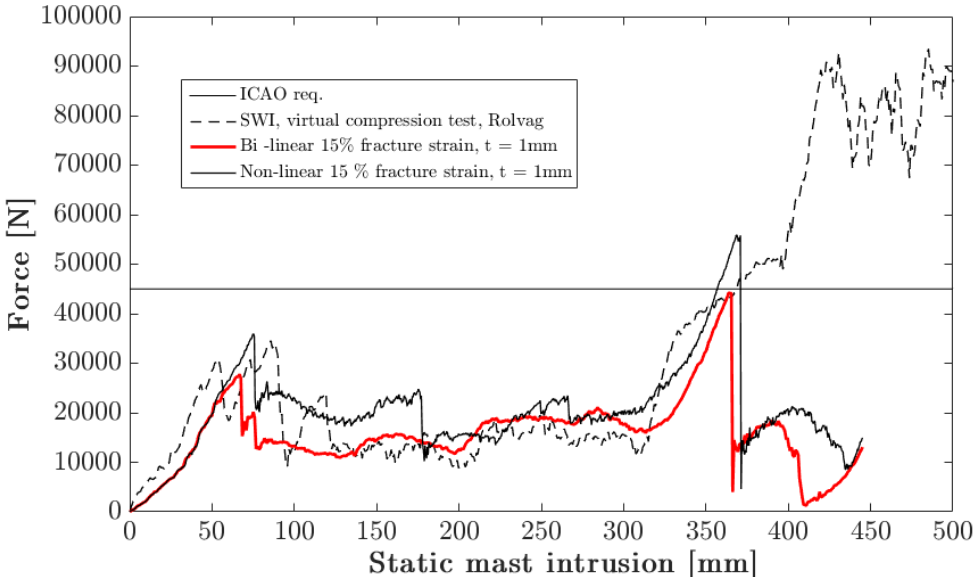


Figure 6.10: Comparison quasi-statical tests.

6.3.2 Dynamic

Four dynamical compression test was performed with an intruder velocity of 140 km/h which is the prescribed ICAO standard. The recorded reaction forces on the intruder’s rigid reference point was filtered using a common 1 kHz low-pass filter. The simulations were stopped just before skin started to stack against the main support tube. As we can see from figure 6.12 and 6.13, both skin thickness gave the same initial deformation and stiffness as the SWI. A skin thickness of $t = 1$ mm yields however much higher reaction forces for both material models prior to skin buckling and failure occurred for both material models, with a peak value of around 40 kN for the non-linear and around 38 kN for the bi-linear. Visual inspection compression showed that the dynamic impact test with a skin thickness of $t = 1$ mm were dominated by a buckling type deformation from buckling of the sidewalls. This was observed for both the non-linear material model and the bi-linear material model. The corresponding dynamical compression forces are as we can see from figure 6.12 and 6.13 oscillating with a much larger range. A skin thickness of $t = 0.8$ mm yields reaction forces in close agreement with the SWI for both material models. The thinner 0.8mm gives as a expected lower buckling forces. At around 250 - 270 mast intrusion, depending on

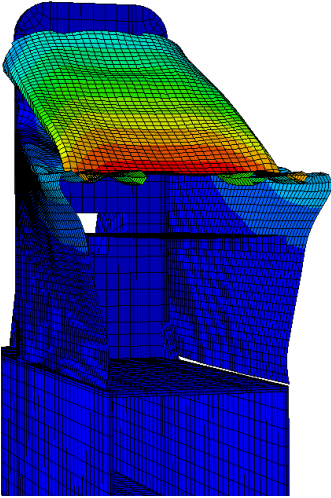


Figure 6.11: Skin regains strength.

the material model, an increase of reaction forces followed by a small drop just before mainspar is hit are observed for both models and thicknesses. This is due to the skin regains strength as shown in figure ???. As we can see from the plots, the surrogate impactors deformation modes were less sensitive to strain hardening, and more sensitive to skin thickness. It is also noted that the force range are in the same levels as the SWI.

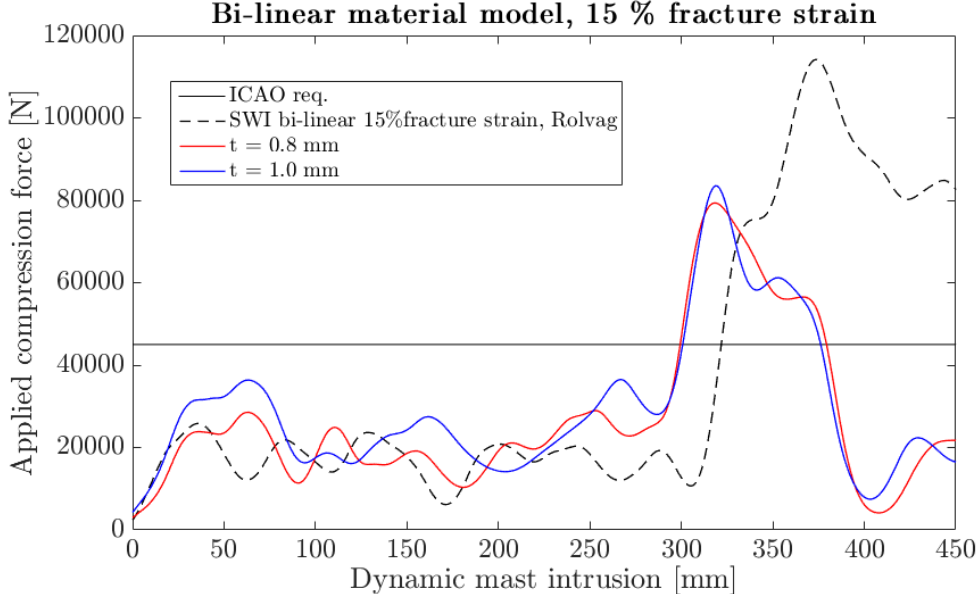


Figure 6.12: Dynamic compression forces, bi-linear material model

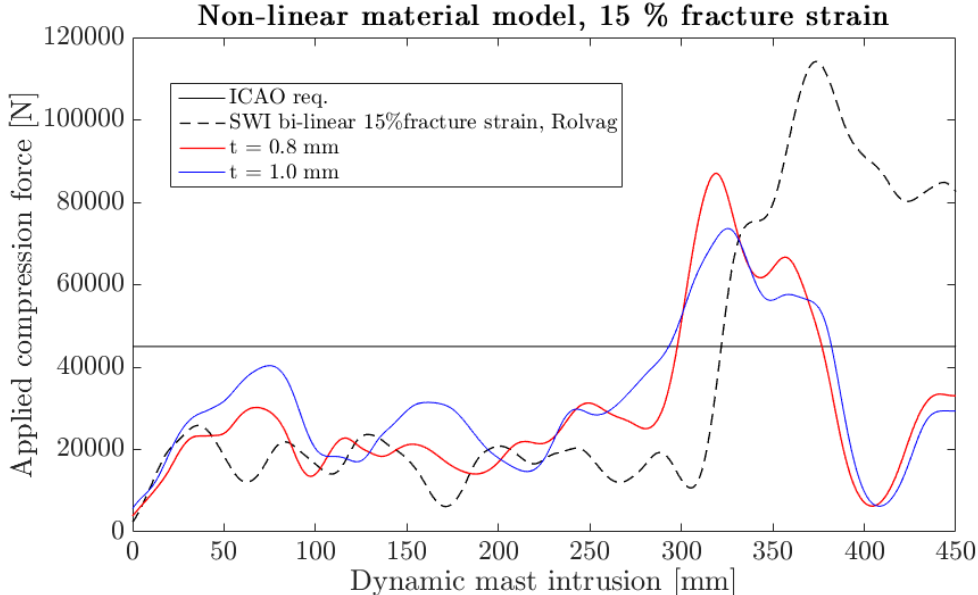


Figure 6.13: Dynamic compression forces, non-linear material model.

6.4 Discussion

The quasi-static compression tests showed that the alteration of skin fixture had an effect on both the recorded peak forces and deformation modes from what was recorded in the conceptual analysis. By fixing the skin at three separated flat regions as opposed to a continuous smooth curved surface lead to unstable failure of the flanges. The unfixed region of the skin, meaning the part which spans over the curved edge of the side-support led to a rapid loss of strength as the flanges failed, as opposed to a more successive loss of strength which was observed in the conceptual principle structure and in the SWI [3]. These effects are however prone to insecurities related to material modeling and the mass scaling of the model may have great effect on the actual response.

The effects observed in the quasi-static analysis were however eliminated when the impactor was compressed in the dynamical tests with an intruder speed of 140 km/h. Furthermore, a skin thickness of 1 mm yielded reaction forces and deformation modes relatable to the SWI in the quasi-static analysis, but gave too high reaction forces in the dynamical analysis for both material models. As it was dominated by buckling type deformation, the forces oscillated at a much lower rate and at higher force-levels for both material models than the SWI. A skin thickness of 0.8 mm gave much lower reaction forces in the quasi-static analysis, and altered the deformation of the impactor. In the dynamical analysis however it was in close agreement with the SWI for both material models. It is noted that the impactor were somewhat insensitive to strain hardening in the dynamical analysis, and skin thickness were therefore the.

The support structure did experience some unwanted deformations prior to skin failure.

Chapter 7

Conclusion and recommendations for further work

In this thesis a simplified and perceived low-cost impactor has been developed

7.1 Conclusion

The project was aimed at developing a new simplified soft impactor for testing of frangible aviation masts. The impactor was aimed at reducing cost, and reinstate the use of a soft impactor in crash analysis of aviation masts. Four different concepts has been presented and tested on a conceptual level. The concept was to mimic the structural response to a wing section of a small aircraft. The winning concept from the conceptual phase was one simplification of the current standard soft wing impactor.

The concept which yielded the most promising results were further detailed to a degree close to production quality. The concept is a semi-reusable impactor, where only two components are replace between testing.

A quasi-static compression test and a dynamical impact test was chosen to investigate the crush characteristics of the new impactor. The tests was done as a FEA, and can only be considered as an indication of the actual response as simple material definition was used. Two material models were chosen to investigate its sensitivity to strain hardening. The results from the quasi-static analysis showed that the crush response deviated some from the one of the current product. It inhibited the same deformation modes, but force-levels were a little low. It also showed that the model was sensitive to different post-yielding strain hardening behaviours.

The results from the dynamical analysis showed that the crush characteristics of the impactor with a skin thickness of $t = 0.8$ mm was in very good relation to the ones currently on the market. The dynamical analysis also showed no sensitivity to strain hardening behaviour. As the tool is to be used in physical high-spded crash testing, these results are considered to be of greater importance. Hence, the proposed solution could be used to simulate the impact of an aircraft wing. Some alterations must be done before this product is put to use however.

A simplified cost analysis has been counducted on the raw-materil use and showed a significant reduction of costs.

7.2 Further work

During the process and after the product development process and final product testing, several areas and elements were discovered which could be further improved:

- Not related to this paper, but the dynamic properties of the SWI must be verified by physical quasi-static compression tests, as this was not the case during this work. The properties and validity of the proposed solution should be evaluated against these results before anything further work is done.
- The support structure in the proposed solution should be optimized before the impactor proposed are to be used. The weight of the support structure alone was twice as much as the entire SWI, which is considered to be way too much. In hindsight, the tubular support-structure gave much greater strength to weight ratio, and could be used favourably with small alterations.
- The decision to use an aluminum plate, suspended between the support structure ribs to generate the characteristic second rise of reaction forces was made due to the perceived cost benefits. This led to a somewhat complicated support structure, due to the large inwards-pulling forces generated on the ribs. A simple self-supporting deformable structure replacing the mainspar could be favourable in order to reduce the complexity and thickness of the side-ribs.
- Mounting the skin with several bolts along the skin was discarded by the author due to the aversion of skin alteration (drilling of holes) and to the perceived tedious task of interchanging the skin between tests (large amount of bolts must be used in order to ensure a smooth transition of skin shearing). As crash tests of frangible aviation masts are performed with a
- The concept with the honeycombs is still considered as an interesting and promising solution to this problem, but was chosen not to further develop in this project. A further investigation with a deeper knowledge and understanding of the crushing behaviour of the honeycombs may further improve this concept. A self-supporting fully-replaceable impactor, obtained from stock with standardized sizes set by the ICAO is one which would drastically reduce the test costs, despite the rather large price of honeycombs.

Bibliography

- [1] M. N. Ensan, “Frangibility analysis of approach lighting composite tower,” Tech. Rep. LTR-SMPL-2009-0120.
- [2] R. Frijns and J. Wiggenraad, “Static compression tests and computer models of wing impactors used for impacts on frangible airport approach lighting towers,” Tech. Rep. NLR-CR-99495, 1999.
- [3] T. Rølvåg, T. Welo, R. van Houten, and J. Wiggenraad, “Fe simulation of soft wing aviation mast impactor - sensitivity to model assumptions.”
- [4] K. T. Ulrich and S. D. Eppinger, *Product design and development*, 3rd ed. McGraw Hill/Irwin, 2007.
- [5] *HexWeb Honeycomb Attributes and Properties*, Hexcel, 11 1999, tSB-120.
- [6] D. Systèmes, “Abaqus analysis user’s manual,” *Simulia Corp. Providence, RI, USA*, 2007.
- [7] J. Wiggenraad, M. van Houten, and C. Rooks, “Development of requirements, criteria and design guidelines for frangibility of structures at airports.”
- [8] “Aircraft accident report pan american world airways, inc., boeing 747, n747pa, flight 845, san francisco, california, july 30,1971,” Tech. Rep. NTSB-AAR-72-17, 1972.
- [9] *Aerodrome design manual, Part 6 - Frangibility*, International Civil Aviation Organization (ICAO), 2006.
- [10] R. W. Harralson, C. W. Laible, and J. Lazarin, “Development and test of low impact resistance structures. volume i. structural and dynamic aspects.” Tech. Rep. FAA-RD-73-187, February 1974.
- [11] E. Rogers, J. Ross, and K. Snyder, “Development and test of fiberglass low-impact resistant towers.” Tech. Rep. No. FAA-AF-79-1, 1979.
- [12] R. Dinan, D. Duke, and C. Rooks, “Airfield frangibility criteria: Questions and concerns with current standards,” October 2014.
- [13] J. Hanka, “Impact tests of exel approach light masts.”
- [14] D. Zimcik and A. Selmane, “A study on the frangibility of airport approach lighting towers - asic-e-98-1 - phase i,” 1998.
- [15] Tech. Rep.
- [16] B. Griffith, “Frangibility impact testing review,” October 2014.
- [17] T. Rølvåg, “Frangibile aviation masts, research questions for my sabbatical year.”
- [18] J. Olthoff, “Impact testing of a full scale frangible approach lighting structure,” Tech. Rep. NLR CR 90239C, 1990.
- [19] J. Doke, “Grabit,” 2007.

- [20] G. Pahl and W. Beitz, *Engineering design: a systematic approach*. Springer Science & Business Media, 2007.
- [21] K. G. Robbersmyr and O. K. Bakken, “Investigation of frangibility for lattix light towers,” 1997.
- [22] F. Irgens, “Formelsamling mekanikk,” *Tapir akademiske Forlag*, 1999.
- [23] F. Doengi, S. Burnage, H. Cottard, and R. Roumeas, “Lander shock-alleviation techniques,” *ESA bulletin*, vol. 93, p. 2, 1998.
- [24] A. Eskandarian, D. Marzougui, and N. E. Bedewi, “Finite element model and validation of a surrogate crash test vehicle for impacts with roadside objects,” *International Journal of Crashworthiness*, vol. 2, no. 3, pp. 239–258, 1997.
- [25] N. E. Dowling, *Mechanical behavior of materials: engineering methods for deformation, fracture, and fatigue*. Pearson Education Limited, 2013.
- [26] R. L. Mott, *Machine Elements In Mechanical Design, fourth edition*. Prentice Hall, 1992.
- [27] R. CHibbeler, “Engineering mechanics: Statics,” 2010.

Attachment 1 - Material prices

			Source Lasaero.com (25.11.2015)			Source aircraftproducts.wicksaircraft.com (25.11.2015)		
<u>Aluminium 2024- T3 0.8 mm sheet:</u>								
	w [mm]	b [mm]	£/plate	NOK/plate	\$/plate	\$/plate	NOK/plate	
4'x2'	1219.2	609.2	30	390.2082	43.69005	44.47	397.1741	
4'x4'	1219.2	1219.2	60	696.6401	78	85.07	759.7842	
6'x4'	1828.8	1219.2	90	1170.625	131.0701	115.97	1035.761	
8'x4'	2438.4	1219.2				139.24	1243.592	
<u>Aluminium 2024- T3: 1 mm sheet:</u>								
4'x2'			39	507.2706	56.79706	52.73	470.9465	
4'x4'			78	1014.541	113.5941	100.88	900.9878	
6'x4'			117	1521.812	170.3912	137.5	1228.051	
<u>Aluminium 2024- T3: 1.63 mm sheet:</u>								
4'x2'			45	585.3123	65.53507	80.54	719.3255	
4'x4'			90	1170.625	131.0701	185.24	1654.431	
6'x4'			135	1755.937	196.6052	177.19	1582.534	
<u>Aluminium 2024- T3: 2.032 mm sheet:</u>								
4'x2'			74	962.5135	107.7688			
4'x4'			147	1912.02	214.0812			
6'x4'			220	2861.527	320.3937			
<u>Aluminium 2024- T3: 2.3 mm sheet:</u>								
4'x2'			74	962.5135	107.7688			
4'x4'			147	1912.02	214.0812			
6'x4'			220	2861.527	320.3937			

Attachment 2 - Risk assessment

NTNU	Kartlegging av risikofylt aktivitet			Utlarbeidet av		Dato	
				HMS	HMS-avd.	Nummer	HMSRV2601
			Godkjent av	Side		Erstatter	
			Rektor			01.12.2006	

Enhet: Institutt for produktutvikling og materialer
 Linjeleder: Torgeir Welø
 Deltakere ved kartleggingen (m/ funksjon): Jørgen Johnsen (student)

Dato: 14.08.2015

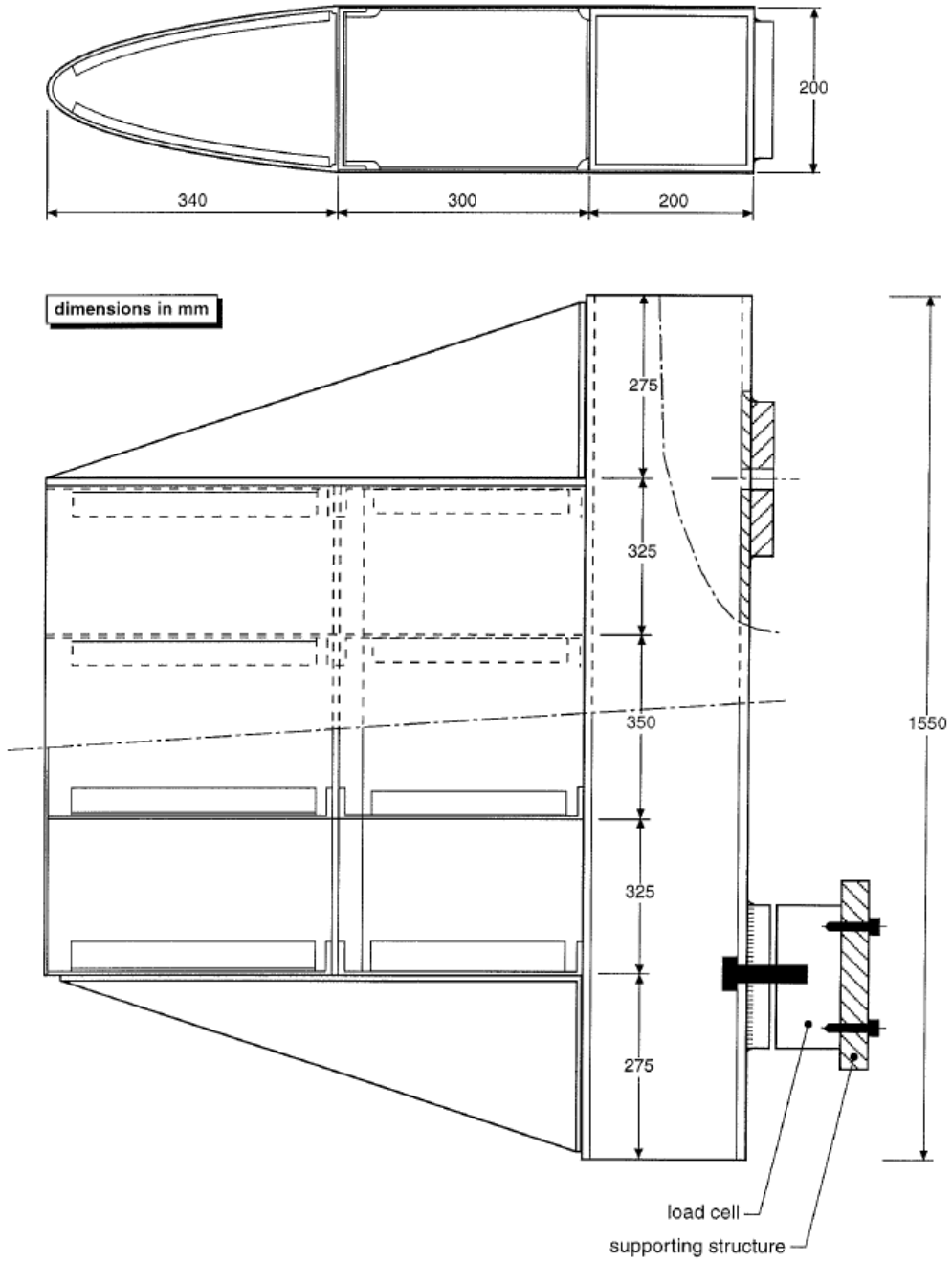
Kort beskrivelse av hovedaktivitet/hovedprosess: Masteroppgave Jørgen Johnsen: Vingepropaganda for testing av flyplass-master.
 Er oppgaven rent teoretisk? (JA/NEI): JA «JA» betyr at veileder innestår for at oppgaven ikke inneholder noen aktiviteter som krever risikovurdering. Dersom «JA»: Beskriv kort aktiviteten i kartleggingskjemaet under. Risikovurdering trenger ikke å fylles ut.

Signaturer: Ansvarlig veileder:  Student: 

ID nr.	Ansvarlig	Eksisterende dokumentasjon	Eksisterende sikringstiltak	LoV, forskrift o.l.	Kommentar
1					
2					

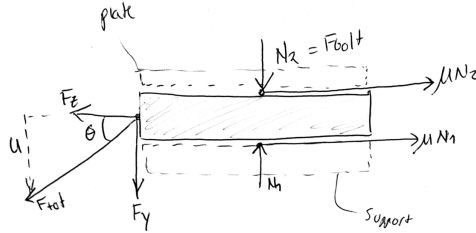
Attachment 3 - Soft wing impactor dimensions

Standard softwing impactor dimensions used in EXEL [13] test programme. Drawing from [2].



Attachment 4 -Bolt load calculation

The clamping loads of the bolts have to be calculated in order to properly fasten the skin to the support structure. A conservative measure of bolt loads, and bolt dimensions are performed for simulation and feasibility reasons. A more detailed calculation must be performed should this product be utilized. By decomposing the total force which acts on the top part of the support structure by the inwards pulling of the skin on impact, as shown in the included figure, we are able to calculate the total clamping force required. If we assume that the plate is completely fixed by the bolt loads, only static frictional forces are present. If we further assume that the theory of dry friction (coloumb friction) are applicable, the bolt loads can easily be calculated. Dry friction acts tangent to the contacting surface, in a direction opposed to the motion (or tendency of motion). Furthermore, dry friction is independent on contact area [27].



The surrogate impactor has a design failure load of 32 \pm 2 kN. Furthermore it should break at around 80-100 mm skin deformation. The impactor is 1000 mm wide and by utilizing these geometrical relations we can calculate the angle of which the force acts on the support structure by $\theta = \tan^{-1}(\frac{2u}{width})$. Where u is the deformation of the skin (100-80/2) and w is the width of the impactor. The angle was calculated to be 10.4 degrees. We can then decompose the forces into F_z and F_y as shown in the included figure by simple sine-cosine and tan relations. By using newton's second law, the bolt individual bolt can be found by:

$$F_{bolt} = \frac{F_z - \mu F_y}{2n\mu}$$

Where n is the number of bolts and μ is the coefficient of friction between the aluminum skin and steel support-structure/pretension plates.

Two measures of the forces has been document, one analytical and one collected from the geometry optimization simulations. The analytical yields $F_y = 17\ 000$ and $F_z = 85$ kN whilst the results from the geometry optimization setup was $F_z = 53\ 000$ kN and $F_y = 7\ 000$ kN. This is a major difference, which may be due to the rather drastic assumption that the top fixture holds all the forces, as is not the case. The forces are also distributed amongst the side-wall fixtures. The results from the simulations are therefore used with a safety factor of 1.5 due to the fact that dynamical forces are expected to be even higher. Two bolt configurations have been considered, as a design requirement it was decided that each bolts was to be stressed to a maximum 75 % of its proof strength:

1. Two bolts: Equation 1 gives us a bolt load of $F_{bolt} = 96750$ kN. If we choose a grade 9.8 steel bolt which has an approximate proof strength of 650 MPa [?] we get an allowable stress of $\sigma_a = 0.75 * (650MPa) = 487.5$ MPa. The required tensile stress area for the bolt is then $A_t = \frac{F_{bolt}}{\sigma_a} = 198.4mm^2$. From table 18-5 page 718 in [?] we can choose M20 coarse thread bolt. This is an unrealistic choise in this design. The alternative is to choose a higher steel grade bolt. Tighening torque [?]: $T = KDP = 290.25$ Nm. A wrench with a length of 20 mm yields a a applied force of 1451 N which is equivalent to lifting 147 kg. This is therefore unfeasible configuration.
2. Four bolts: $F_{bolt} = 64.5kN \Rightarrow A_t = 132.3mm^2$. From the same table, we choose an M16 bolt. The required tighening torque will be $T = 154,8$ Nm. Approximately half the torque as in 1) but

Attachment 5 - Surrogate wing impactor dimensions.

